DIPLOMA THESIS

Interface design of arc-evaporated Aluminium-Chromium-based oxynitride coatings

by

Maximilian Palir
1227034
Braunhubergasse 25-29 5/5 1110 Wien

carried out for the purpose of obtaining the degree Master of Science
under supervision of

Univ.Prof. Dipl.-Ing. Dr.mont. Paul Heinz Mayrhofer
Univ. Ass. Dipl.- Ing. Dr. techn. Helmut Riedl

Institute of Material Science and Technology,
Thin Film Materials Science Division

submitted at

Technische Universität Wien
Getreidemarkt 9/E308-01
1060 Wien

Wien, June 2019

This work was supported by Plansee Composite Materials GmbH and
Oerlikon Balzers Surface Solutions AG in the framework
of the Christian Doppler Laboratory for Application Oriented Coating Development.

Affidavit:
I declare in lieu of oath, that I wrote this thesis and performed the associated research myself, using only literature cited in this volume.

Date *Signature*

Acknowledgements

First, Robert, I would like to thank you for the opportunity to accomplish this thesis under your supervision, and for guiding me through the process. I immensely enjoyed working with such a kind and cheerful person, and your scientific expertise helped me to understand the ongoing process and relations between the results. Thank you for your patience and support!

I would like to especially express my sincerest gratitude to Univ.Prof. Dipl.-Ing. Dr.mont. Paul H. Mayrhofer, for giving me the chance to write my thesis in his research group, and for allowing me to start so soon after obtaining my Bachelor's degree. It was a pleasure to work as part of the group you lead so admirably.

Additionally, I want to thank all the other members of the thin film group, for creating such a welcoming atmosphere and all the support I received. Special thanks to Helmut, for taking over my supervision after Robert finished his thesis, and for all the hours put into proofreading.

Furthermore, I want to thank my family, for the continuous encouragement and the support I experienced throughout my whole life.

The science of today is the technology of tomorrow.
Edward Teller

Contents

List of Figures

List of abbreviations and symbols

AlCrN	$Al_xCr_{1-x}N$
AlCrO	$(Al_xCr_{1-x})_2O_3$
DSC	Differential Scanning Calorimetry
SEM	Scanning Electron Microscopy
EDX	Energy Dispersive X-Ray Spectroscopy
PVD	Physical Vapour Deposition
CVD	Chemical Vapour Deposition
CAE	Cathodic Arc Evaporation
DTA	Differential Thermal Analysis
TGA	Thermal Gravimetric Analysis
XRD	X-Ray Diffraction
FEG	Field Emission Gun
SE	Secondary Electrons
λ	wavelength of irradiating light
n	natural number
d	lattice spacing
θ	angle of incidence
G	Gibbs free energy
H	enthalpy
S	entropy
T	temperature
H_{AB}	enthalpy of the bonding between species A and B
H_{AA}	enthalpy of the bonding between species A and A
H_{BB}	enthalpy of the bonding between species B and B
ΔG_{mix}	Gibbs free energy for mixing of species
ΔH_{mix}	enthalpy for mixing of species
ΔS_{mix}	entropy for mixing of species
J	flux of particles
D	diffusion coefficient

c	concentration
t	time
Γ	jump frequency
ΔG_m	free activation enthalpy for migration
R	gas constant
α	jump distance
Δm	mass gain
A	total sample surface
k_p	parabolic oxidation constant
Δs	increase in oxide layer thickness

Abstract

Physical Vapour deposited $Al_xCr_{1-x}N$ and $(Al_xCr_{1-x})_2O_3$ tool coatings are nowadays commonly used for machining applications to improve the overall tool performance, most notably the hardness, wear resistance, and thermal stability. As recently shown by former studies, architectural design of $Al_xCr_{1-x}N/(Al_xCr_{1-x})_2O_3$ multilayer coatings is a way to further improve the mechanical properties within these oxynitrides. Starting from this point, it was now the goal to investigate the influence of the coating composition on the thermal stability and oxidation resistance of these coatings. For this purpose, coatings with different $Al_xCr_{1-x}N/(Al_xCr_{1-x})_2O_3$ ratios were deposited and tested. High temperature analyses of the ground, powdery coatings showed increasing oxidation resistance with higher oxygen content of the coating. The temperature stability data obtained within these tests were used to develop an experimental procedure to investigate the oxidation stability of the samples in their natural, as deposited form. The long-term furnace annealed samples were examined using a scanning electron microscope equipped with an EDX (Energy Dispersive X-Ray Spectroscopy) detector for executing line scans via the specimen cross section. The results from this experiment completely contradicted the trends observed during the other experiments, as the high nitrogen content coatings now easily outperformed the high oxygen content coatings. Considering these findings, it has to be deduced that higher $(Al_xCr_{1-x})_2O_3$ content is not necessarily a cause for higher oxidation resistance, but, quite contrary, the stability seems to decrease with higher percentage of $(Al_xCr_{1-x})_2O_3$ in the coating. This does, however, not mean, that intermixing of $(Al_xCr_{1-x})_2O_3$ and $Al_xCr_{1-x}N$ layers has a negative influence on oxidation resistance. With the results at hand, it should suffice to say that, according to our research, oxidation stability of $Al_xCr_{1-x}N/$ $(Al_xCr_{1-x})_2O_3$ in as deposited form increases with decreasing oxygen content in the coating within the investigated spectrum.

Kurzfassung

PVD (Physical Vapour Deposition) ist eine Standardmethode zur Erzeugung von harten, verschleißfesten und temperaturbeständigen Werkzeugbeschichtungen. Unter diesen zeichnen sich, wie von vorausgehenden Studien gezeigt, viellagige Strukturen aus abwechselnden Schichten von $Al_xCr_{1-x}N$ und $(Al_xCr_{1-x})_2O_3$ durch besonders gute mechanische Eigenschaften aus. Das Ziel dieser Arbeit besteht in der Untersuchung der thermischen Stabilität, sowie der Hochtemperatur-Korrosionsresistenz dieser Beschichtungen. Zu diesem Zweck wurden Beschichtungen mit unterschiedlichen Mischungsverhältnissen von $Al_xCr_{1-x}N$ und $(Al_xCr_{1-x})_2O_3$ abgeschieden und deren Leistungsvermögen getestet. Mittels Analysen bei erhöhter Temperatur in Helium - und Sauerstoffatmosphäre konnte ermittelt werden, dass die Stabilität der zu feinem Pulver vermahlenen Schichten mit erhöhtem Gehalt an sauerstoffreichen Lagen zunimmt. Auf Basis der Ergebnisse dieser Untersuchungen wurde eine Testprozedur zur Ermittlung der Oxidationsresistenz der Beschichtungen in ihrer ursprünglichen, unvermahlenen Form entwickelt. Diese sollte die Entwicklung der Probeneigenschaften nach längerer Verwendungsdauer abbilden. Die Begutachtung der Teststücke erfolgte mithilfe eines Rasterelektronenmikroskops (SEM), wo die Probenquerschnitte linienförmig mittels energiedispersiver Röntgenspektrometrie (EDX) abgetastet wurden. Die erhaltenen Ergebnisse widersprachen den Resultaten der anderen Experimente. Die thermische Beständigkeit der Beschichtungen stieg mit sinkendem Sauerstoffgehalt. Da die Messwerte des letzten Versuches das reale Einsatzgebiet aufgrund der Verwendung in abgeschiedener Form am besten abbilden, muss geschlossen werden, dass ein höherer $(Al_xCr_{1-x})_2O_3$ - Anteil nicht zu einer Verbesserung der Eigenschaften von $Al_xCr_{1-x}N$/ $(Al_xCr_{1-x})_2O_3$ Multilagenbeschichtungen führt. Zumindest im Betrachteten Mischungsbereich ensteht durch die vermehrte Verwendung von $(Al_xCr_{1-x})_2O_3$ in der Beschichtung keinen Vorteil hinsichtlich der thermischen Beständigkeit.

Chapter 1

Introduction

During the last centuries, scientific findings and technological developments were the mayor driving forces behind the evolution of our society. Well-grounded knowledge in the field of mechanics and physics, combined with new materials, enabled a new way of designing machines fit to fulfil our requirements. With the emergence of assembly line production, at the latest, the need for cheap, accurate and, most importantly, fast manufacturing became of paramount importance. All our advances in technological fields are closely connected to our ability to generate increasingly complex parts with high accuracy, while costs are steadily decreased. High precision tool cutting is one of the most important fabrication methods, used every second around the world in service of the production of high quality goods, ranging from final machining of mass use articles (e.g. ball bearings) to extremely specialised high performance products for prosthetics or space travel, just to give some examples.
From the development point of view, cutting tools require a diverse set of characteristics that are often contradictory and hard to fulfil with one single material. Lathe chisels and milling cutters have to hold a hard, sharp cutting edge, while still being ductile enough to withstand transient loads without failure. Additionally, the tools need to be highly temperature resistant, so that high cutting speeds can be achieved. Especially stability against high temperature oxidation is of crucial importance. The vast majority of cutting operations happens in standard atmosphere, so that oxygen can freely access the tool surface. Species prone to oxidation are therefore highly dubious candidates for tool coatings for standard (non-vacuum / non-inert gas) applications. Lowering the tool wear, translating to an increased tool life, is also highly desirable. Continuous improvement in this field have led us to the current state-of-the-art tools, which in general consist of a hard, wear resistant material that can ideally withstand harsh and fluctuating mechanical loads at elevated temperatures. These specifications can be met best by a combination of different materials. Most machining tools used at present consist of a comparatively ductile core, which is coated with a hard, ceramic thin film that further enhances mechanical and thermal resistances and hence overall tool performance [11]. Multiple different material systems are

used as tool coatings, most prominently among them are probably TiN and TiAlN coatings in combination with high speed steel (HSS) or hard metal components. Those coatings can be generated with physical vapour deposition (PVD). This is especially beneficial for tools from HSS, because the deposition temperature of PVD processes typically does not exceed $400°C$([5, 12, 13]). For the performance of machining tools, one of the most important characteristics is the maximum application temperature, at which the tool can still endure the typically harsh conditions. A higher maximum temperature drastically increases the productivity of machining, because higher cutting speeds and shorter cool-down periods can be realized. Finding new coating compositions with better characteristics has been the cause for extensive research. $(Al, Cr)N$ and $(Al, Cr)_2O_3$ systems, which will in continuation be referred to as AlCrN and AlCrO systems, have shown good performances in this regard. While AlCrN exhibits better mechanical properties, AlCrO typically shows higher oxidation resistance. Furthermore, it is known [10, 14] that mechanical properties can be increased by designing a layered coating architecture. On this basis, it was decided that AlCrN/AlCrO multilayer coatings should be further investigated. The scope of this thesis is to cover the influence of the AlCrN/AlCrO ratio within the coating on thermal - and oxidation stability.

Chapter 2

Theoretical background

In this chapter, a short overview on the basic knowledge in the field of material science, required to understand the further work, is given. Material science is a scientific field as old as humanity itself. In fact, we even name the first historical eras where humans roamed our world after the materials they used to build their tools, such as stone age and bronze age. The further our understanding of our surroundings and our craftsmanship evolved, the more diverse and complicated became the materials we used. During our history material science changed from pure selection in the early stages, via slight modification by combining different substances, to a fundamental understanding of the material structure on the atomic scale. This understanding nowadays enables us to tailor materials specifically fulfilling our needs. Nonetheless, a lot of research is still necessary to identify promising materials, meeting our expectations concerning enhanced performance. The constantly expanding number of different thin film coatings and the steady emergence of new application fields offer a great example for the progress in material science [10, 15].

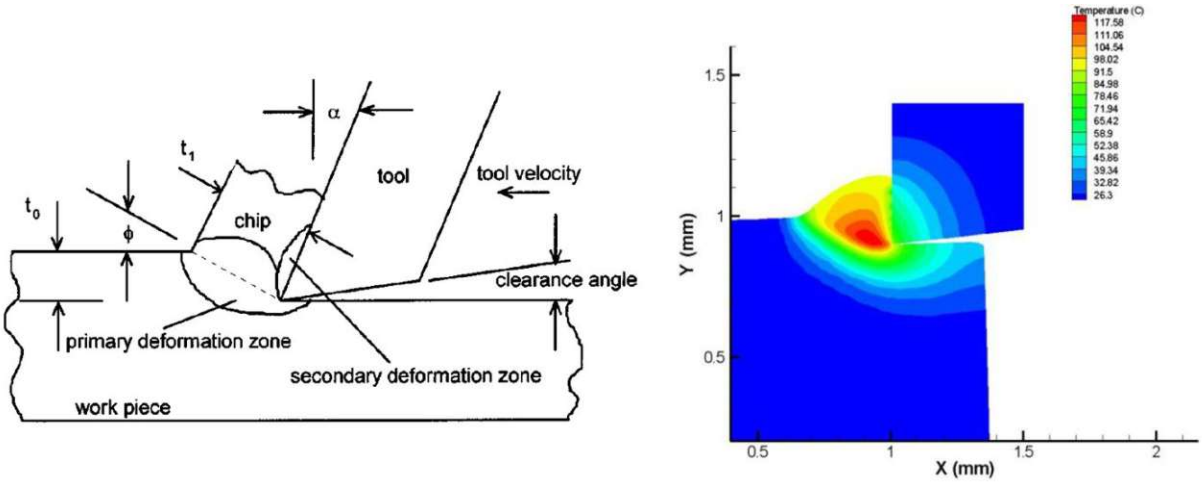

Figure 2.1: Image of the cutting process [1], Temperature field during the cutting operation [2]

2.1 Material properties

Material properties can be classified regarding the chemical, thermal, optical, mechanical, electrical, etc. properties. It is the goal to sculpt materials with very good performance in the desired characteristics that additionally do not suffer from mayor drawbacks in less important material properties. Therefore material development is always an act of balancing drawbacks and benefits. The major properties required for cutting tools are excellent thermomechanical performance, e.g. hardness and wear resistance, while also maintaining sufficient toughness and resistance against brittle material failure. fig. 2.1 depicts the cutting operation with all its parameters and the temperature distribution during the cutting process.

The tool moves with the tool velocity relatively to the work piece. The forces and temperatures acting on the chisel are a function of this velocity and the depth of cut t_0. The tool geometry plays an important role for the removal of chips from the cutting area. To achieve a high productivity, the depth of cut and the tool velocity should be maximized. This necessitates good mechanical properties (hardness, stiffness and strength) as well as the ability to withstand elevated temperatures. Ceramic coatings like TiN or $(Al_xCr_{1-x})_2O_3$ can comply with those demands due to their high melting points and their elevated oxidation resistances. Additionally, the low thermal conductivity helps to shield the tool core from high temperatures, as visible in fig. 2.1 [1, 2, 11, 16]. The internal part of the tool serves as a substrate for the coating, while also providing the necessary mechanical support and a much higher ductility than the coating. This prevents brittle failure of the tool.

2.2 Deposition techniques

The two main techniques used to deposit thin films are Chemical and Physical Vapour Deposition, henceforward referred to as CVD and PVD, respectively. Those two processes are fundamentally different and each has its own advantages. CVD is, as the name implies, a purely chemical process. Anorganic precursors in gaseous state, consisting, in most cases, of halogenides of the desired metallic coating compounds, e.g. $TiCl_4$ for TiN, undergo a chemical reaction. The solid reaction product nucleates and forms a growing layer on the desired surface, while the volatile side-products exhaust as waste [10]. This reaction requires high temperatures of typically more than $800°C$ to provide the necessary activation energy [7]. Therefore CVD can not be used to coat temperature sensitive substrates, such as high performance steels or aluminium alloys. The main advantage of CVD is the high film growth rate, while the need to use gaseous starting substances restricts the applicability. PVD, on the other hand, can be used to apply a wide range of different anorganic (and some organic) substances to various substrate materials. The relatively low deposition temperature additionally allows for the use of temperature sensitive substrates [5, 9, 17, 18]. Generally speaking, all PVD processes follow the same three steps of film formation [7]:

- transition of the source material from liquid or solid state to the vapour phase by physical mechanisms
- transport of the vapour from the source to the substrate
- condensation and subsequent film growth on the substrate

All of these mechanisms can be controlled independently during the PVD process. Depending on the physical principle used to form the vapour phase, PVD is classified into three different techniques: arc evaporation, sputtering, and ion plating. In any case, the vaporisation is carried out by the use of a plasma discharge. Therefore it is most suitable for further explanations to give a general explanation of the main characteristics of plasma. Plasma is a collective, quasi-neutral medium (gas) containing both charged (anions, cations, electrons) and neutral (atoms) particles. Local movements of charged particles result in the formation of dynamic electric and magnetic fields [10]. The schematic model of a plasma chamber can be found in fig. 2.2. Working gas is released into an evacuated chamber. The gas molecules are ionized due to the electric field between the anode and the cathode, which is also called target. The ionized particles enable an arc discharge between the two electrodes. The ionized particles of the plasma are accelerated towards the target, where metal atoms are knocked out by the impact. The gaseous metal deposits on the substrate, which is a ground potential.

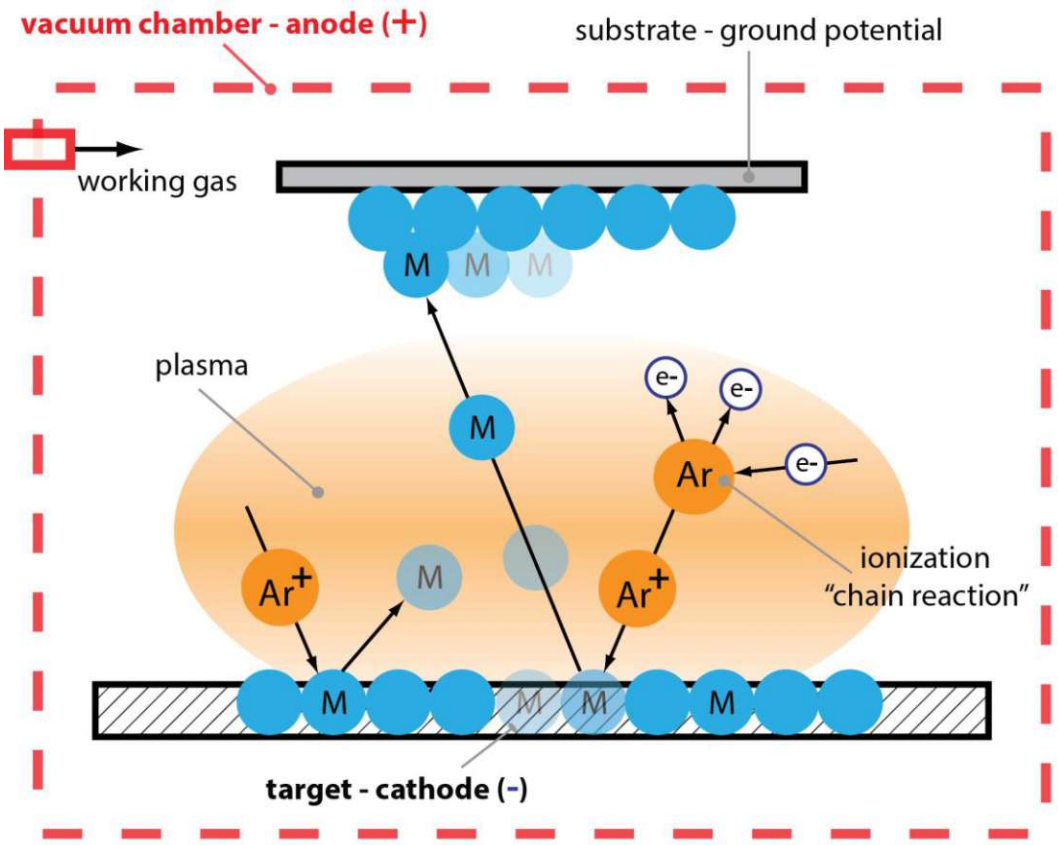

Figure 2.2: Schematic plan of a plasma chamber [3]

We distinguish between three plasma states, namely dark discharge, glow discharge, and arc discharge, which can be characterised via the relationship between voltage and current during plasma formation (fig. 2.3).

The initial stage of plasma formation, A to B in fig. 2.3, is characterised by a current increase when external voltage is applied between a cathode and an anode. The current increase originates from the attraction of background electrons and ions, until point B is reached. At this point, all available particles are attracted. A significant increase in voltage is necessary to provide enough energy for the ionisation of gas particles by cascade-like collision processes. The produced ions are accelerated towards the cathode and lead to an increase in current. Section A to E is called "dark discharge" because of the lack of visible light emission during the process. A so-called dark discharge needs an external electron source to maintain a stable plasma. Beginning at point E, secondary electrons are emitted from the cathode due to ion and photon impact. These electrons lead to a heavy drop of voltage and current amplification. Furthermore, the now autonomously produced electrons stabilise the plasma. The current increase from F to G occurs because the plasma expands over the whole cathode. At H, the glow discharge region ends and thermally induced electron

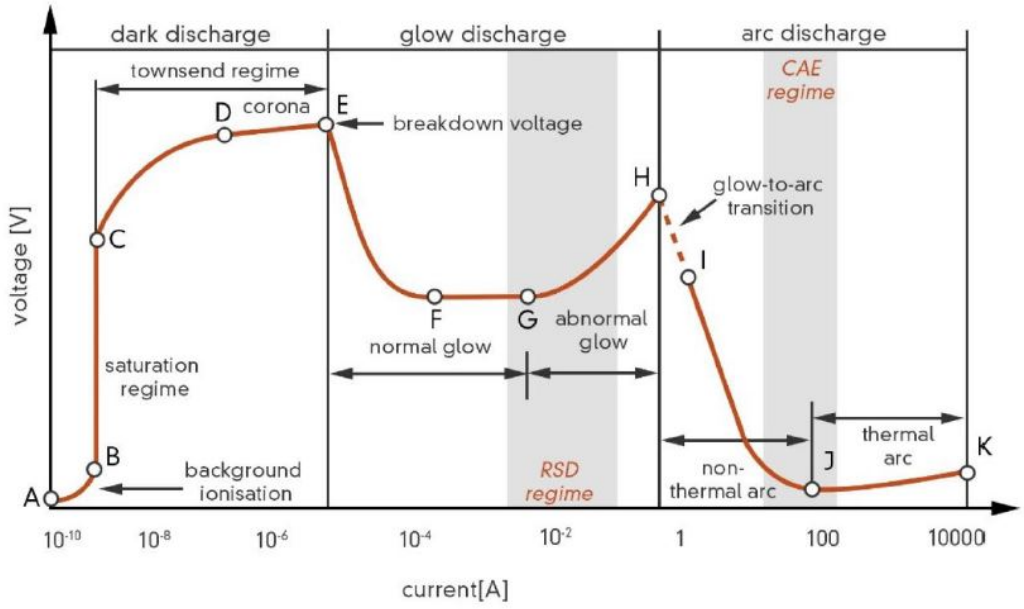

Figure 2.3: Voltage-current relationship during plasma formation [4]

emission occurs at the beginning of the arc discharge region. In this region, as the name indicates, the conditions are dominated by a high current, low voltage arc discharge between the anode and the cathode. A more in-detail explanation will be provided in the following chapter. [4, 7, 10].

2.3 Cathodic arc evaporation

The investigated coatings were produced with Cathodic Arc Evaporation (CAE), hence this technology will be explained in more detail. CAE takes place in the arc discharge region and is one of the main PVD technologies used for industrial applications like drill-or forming tool coatings. The main advantages in comparison to other PVD technologies are namely the high deposition - and ionisation rate. The arc discharge process is initiated by spark generation at the target material surface, representing the cathode. The high degree of ionisation (typically exceeding 90% in comparison with e.g. 5% for sputtering) is the result of a significantly higher power input with regard to a small area, the so called "cathodic spot". This cathodic spot exists only for nanoseconds, during which localized temperatures of about $15000°C$ are reached. This results in a jet of vaporized target material exiting the cathode, leaving behind a crater on the surface. In continuation, the arc reignites nearby the original crater. Thereby, targets covered with non-metallic layers show different spot evolution than purely metallic targets. The arc movement is random by nature, but can be influenced by the application of external magnetic or electric field. This steering results in lower exposure time of individual cathode spots to the arc, and thus to smaller droplet size.

The cathodic arc evaporation process naturally leads to consumption of the cathodic material, known as cathode erosion. During the coating process, two main mass loss mechanisms are observed:

- material leaving the target in vaporised state
- material leaving the target as molten or half-molten droplets

The formation of droplets is caused by the localised melting and vaporizing of the target material. The plasma pressure pushes the molten target material radially outwards, leading to the formation of molten droplets leaving the target at angles typically below 45°., see fig. 2.4. These droplets also reach the substrate, where they are incorporated into the growing film. This is a major disadvantage of the CAE process, because droplets lead to inhomogeneous surfaces, porous coatings and overall lower coating quality. The size and distribution of the particles is mainly dependent on the cathode material. The shape of the droplets is determined by the melting temperature of the target material. On the one hand, metals with low melting temperatures, such as aluminium, are generally still liquid when they hit the substrate. Therefore, a flat, pan-cake like shape is generated. On the other hand, target materials with higher melting temperature, such as chromium, already solidify during flight and are incorporated into the coating as spherical macro-particles. Especially the latter droplet shape is disadvantageous for the coating quality. While the shading effect of surrounding area is quite small for pan-cake like droplets of lower melting components,

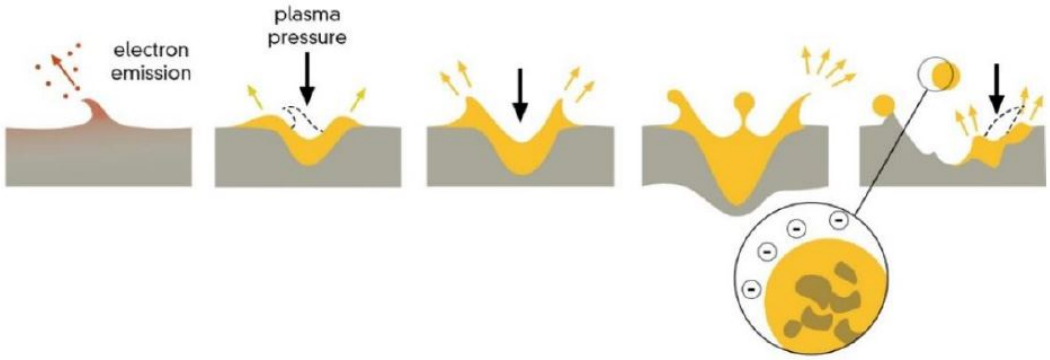

Figure 2.4: Droplet generation during the CAE process due to local plasma pressure on the pools of molten cathode material [4]

it is generally more pronounced for spherical droplets. This leads to a lower density of the coating in the near vicinity of those droplets, and therefore to a lower stability against oxidation processes. [5, 7, 10, 17, 18].

2.4 Growth of cathodic arc evaporated films

For the understanding of thin film coating properties, it is essential to know about the influences film growth has on the coating parameters. One and the same chemical composition can exhibit fundamentally different film properties as a result of diverging film growth. Additionally, it is necessary to discuss the adjustable parameters which allow us to take influence on the film characteristics as well as the chosen deposition parameters for the specimen investigated in this thesis. However, at first, I would like to give a quick overview concerning the thermodynamics of film growth and phase stability.

2.4.1 Phase stability

Stability in a thermodynamic sense is always described by a local or global minimum of energy. This energy, commonly known as Gibbs free energy, is given by the following formula:

$$G = H - TS \tag{2.1}$$

Where H represents the enthalpy, S the entropy and T the absolute temperature. As previously stated, the driving force for every process is the minimization of this Gibbs free energy. This can be achieved by getting to the global minimum, but also by reaching a local minimum. In this case, one would speak of a metastable state. Metastable states are very common in PVD deposition, because the high cooling rate favours their formation. When PVD coatings are exposed to e.g. higher temperatures, decomposition of this metastable coatings into stable products can happen, This can be desired and enforced by post-deposition annealing, or occur due to normal use of the coated product.

Most technically used PVD-coatings consist of several different atoms. Molecular bonds between different atoms only form if they are energetically more desirable than the bonds between atoms of the same kind. We can define the mixing enthalpy ΔG_{mix} as

$$\Delta G_{mix} = G_2 - G_1 < 0 \tag{2.2}$$

while the corresponding enthalpy and entropy can be described by

$$\Delta H_{mix} = H_2 - H_1 \tag{2.3}$$

$$\Delta S_{mix} = S_2 - S_1 \tag{2.4}$$

If we consider a binary system AB, the mixing enthalpy ΔH_{mix} is given by

$$\Delta H_{mix} = H_{AB} - \frac{1}{2}(H_{AA} + H_{BB}) \tag{2.5}$$

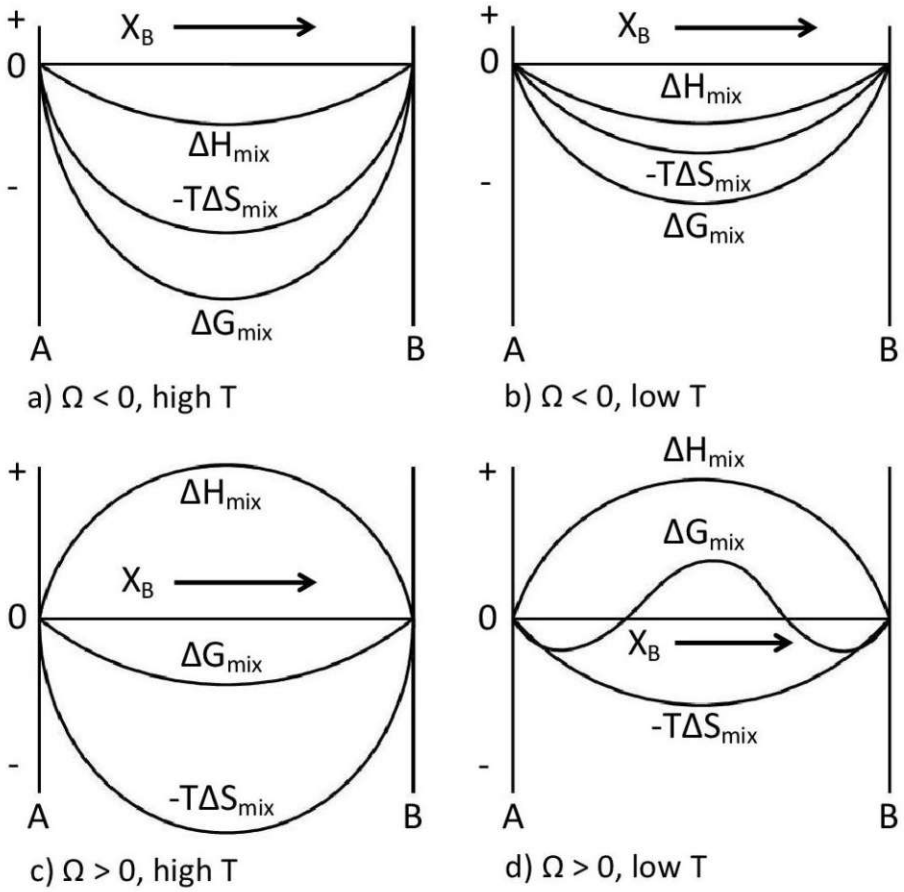

Figure 2.5: Energy diagrams for positive and negative ΔH_{mix} at two different temperatures [5]

where H_{AB} is the enthalpy of the bonding between species A and B, and H_{AA} or H_{BB} describe the bonding between two atoms of the same species, respectively. For ΔG_{mix} to be negative in a system with two species, two options are possible: If ΔH_{mix} is negative, all values of ΔG_{mix} are negative and temperature-independent, as $\Delta S_{mix}$is always negative (fig. 2.5: a,b). If ΔH_{mix} is positive, bonding between Atoms A and B occurs only when the mixture is heated, so that the term $\Delta S_{mix}T$ cancels out the influence of ΔH_{mix}(fig. 2.5: c,d) [5, 10, 15, 19].

2.4.2 Nucleation

Phase transformation is generally initiated by nucleation. This nucleus may henceforward shrink, if the energy gain is smaller than the necessary energy, or grow, which leads to the formation of a new phase emanating from the newly formed nucleus. Energetically speaking, two main contributions to the overall nucleation energy have to be considered. On the one hand, the formation of a new phase has to be thermodynamically favoured in comparison to the existing phase, which means that the Gibbs free energy of the new phase has to be

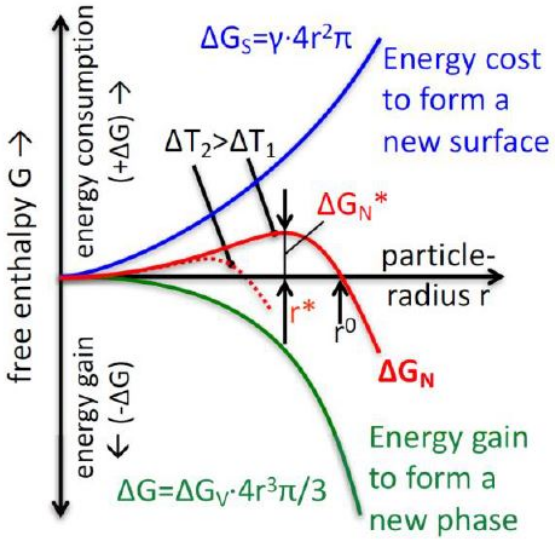

Figure 2.6: Energetic contributions of surface free energy and energy gain due to formation of a new phase to the kinetics of nucleation [6]

lower than the energy of the existing phase. On the other hand, the formation of a nucleus or, respectively, a new phase, increases the surface free energy of the system. This energy increase inhibits the nucleation, and the nucleus can only grow once the contribution of the energy gain from forming a new phase exceeds the energy loss from forming a new surface (fig. 2.6) [5, 15, 19].

2.4.3 Film growth

Film growth, always originating from a stable nucleus, follows its own distinct rules, targeted at the minimum possible energy state. Film growth can be approximated by three different growth modes. The first mode, described by *Frank* and *van der Merwe*, is known as layer-by-layer growth. It occurs if the bonding between substrate and film is stronger than the bonding between the film molecules itself and if high diffusion rates are possible (fig. 2.7: a). Layer-by-layer growth leads to (often preferred) high density films but unfortunately is quite slow. The exact opposite is the second, or island growth mode, as described by *Volmer* and *Weber*. Island growth dominates if the bonding between film atoms is energetically preferable to bonding with the substrate and if energy input does not allow for fast diffusion(fig. 2.7: b). *Stranski-Krastanov* or mixed growth mode is the third approximation model and the one that is most often applicable to PVD coatings. It combines the first two growth modes and features Initial layer-by-layer growth, which may then be followed by the formation of three-dimensional islands, fig. 2.7: c [7, 10].

Figure 2.7: The three growth modes as approximation for real film growth; from left to right: film growth - island growth - mixed growth mode [7]

2.5 Diffusion

Diffusion is the dictating mechanism for almost all high temperature processes. High temperature phase changes and chemical reactions are all based on the faster movement and transposition of atoms. Diffusion driven by an invariable concentration gradient, also called stationary diffusion, can be described by Fick's first law:

$$J = -D\frac{\partial c}{\partial x} \tag{2.6}$$

Instationary diffusion, implying that the diffusion gradient is variable during the diffusion process, is the far more common kind of diffusion process and generally described by Fick's second law.

$$\frac{\partial c}{\partial t} = D\frac{\partial^2 c}{\partial x^2} \tag{2.7}$$

J, the flux of particles, is dependent on the concentration gradient $\frac{dc}{dx}$ and the diffusion coefficient D, which is dependent on multiple process parameters, in solids mainly temperature and activation energies. For diffusion in solids, atoms have to move stepwise from one lattice position to the next position. Atoms have to break the bonds to their neighbours in order to be able to undergo diffusion. this requires a certain amount of energy, the free activation enthalpy for migration ΔG_m. At low temperatures, only few atoms exhibit enough energy to break their bonds, but the diffusion rate increases with temperature. The jump frequency Γ can in general be described as:

$$\Gamma = e^{\frac{-\Delta G_m}{RT}} \tag{2.8}$$

Where R is the gas constant and T the absolute temperature. Depending on the actual diffusion mechanism, the equation may need additional multiplicative factors describing e.g. the concentration of vacancies in the lattice for vacancy diffusion. In any case, the diffusivity D can be derived from the jump frequency and the jump distance α the following way:

$$D = \frac{1}{6}\alpha^2\Gamma \tag{2.9}$$

The two most important diffusion mechanisms in solid bodies are interstitial and vacancy or substitutional diffusion. Interstitial diffusion (fig. 2.8, A) takes place if the atoms of the diffusing species are much smaller than the lattice atoms. In solid chemical compounds, if the atom radii are very unequal, the smaller atom usually occupies interstitial sites in the lattice built up by the bigger atoms. Interstitial diffusion happens between these interstitial sites. Vacancy diffusion (fig. 2.8, B) is the main mechanism for diffusion in lattices of same-sized compounds or single component crystals. Atoms interchange lattice places by jumping from lattice vacancy to vacancy. Naturally, the vacancy concentration has a crucial influence on the speed of vacancy (or substitutional) diffusion.

In general, interstitial diffusion is much faster than substitutional diffusion because normally the number of interstitial sites is much higher than the number of lattice vacancies. Additionally, lattice atoms are bigger than interstitial atoms and therefore show slower diffusion.

The previous explanations clarify the diffusion mechanisms in single-crystalline bulk material. However, real materials normally consist of multiple small crystal grains and show interfaces, free surfaces and dislocations. These imperfect crystalline structures allow for high diffusivity path diffusion, because ion or atom movement is much easier along defective lattices. Diffusion using these pathways typically is 1 to 2 orders of magnitude faster than diffusion in bulk material and allows for various effects such as stress relaxation or even rain growth and recrystallisation. Due to the nature of the PVD process, PVD coatings contain a high number of defects such as grain boundaries, dislocations or vacancies, and interstitial atoms. This has two major effects on the coatings performance: on the one hand, the high defect density leads to better mechanical properties because the dislocation movement is impeded. On the other hand, the elevated application temperatures of often up to $700 - 1000°C$ lead to amplified diffusion along the high diffusivity pathways. This obviously causes changes in the material structure that have to be considered and may even be a major reason for failure. Especially the use under corrosive atmospheres such as high oxygen content gases (e.g. air) is prone to cause the fast destruction of the coating by complete oxidation [5, 15, 20].

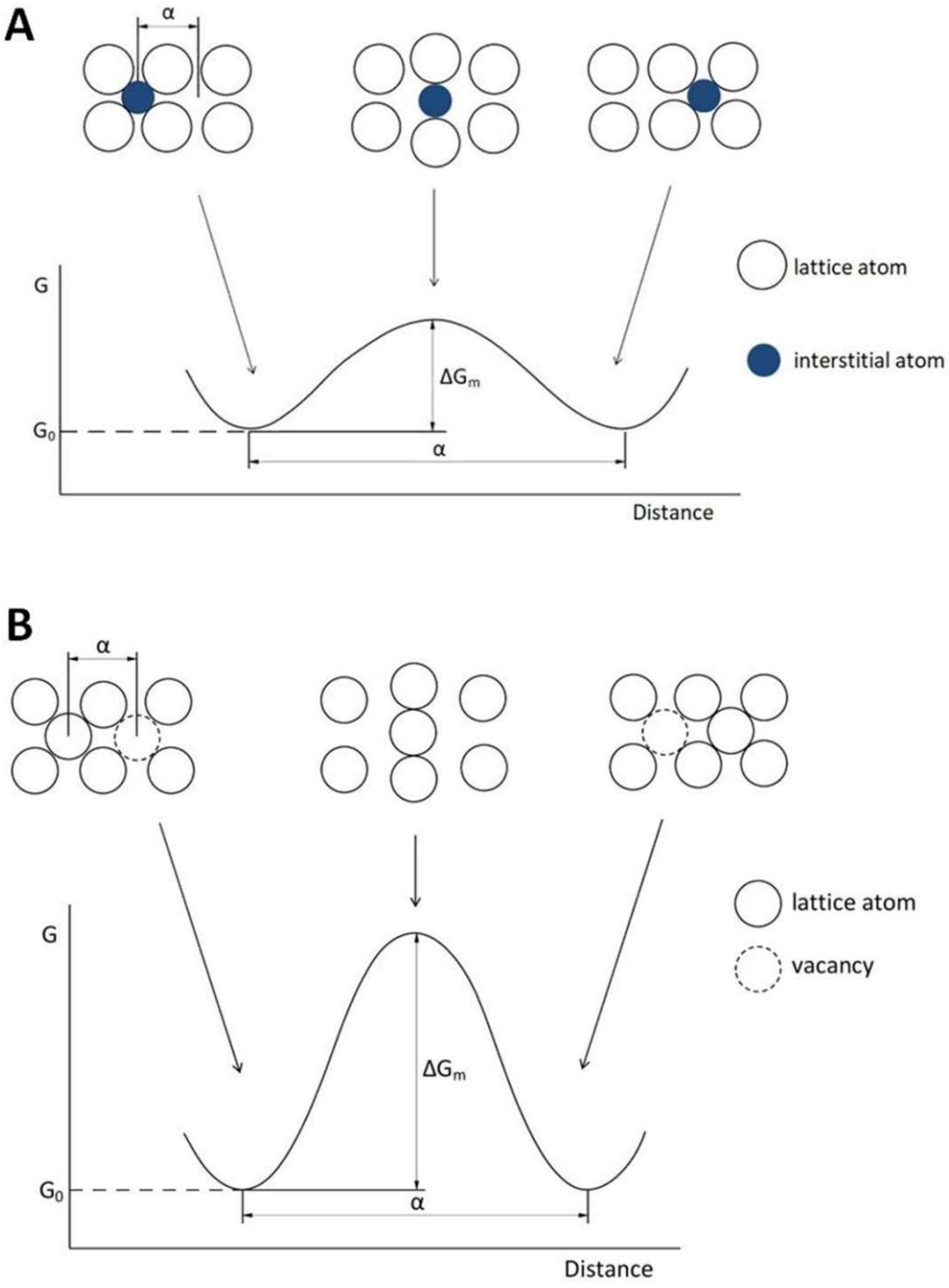

Figure 2.8: Energy diagram and mechanism for interstitial diffusion (A) and for vacancy diffusion (B) [5]

2.6 Oxidation

Oxidation, in general, refers to the exchange of electrons between two different atomic species, one being the oxidant while the other is called reducing agent. Starting from two uncharged atomic species in their natural state, the oxidant takes the electron provided by the reducing agent, resulting in the formation of two charged species. The now negatively charged atom, the oxidant, has been reduced by the reducing agent, while the reducing agent was oxidised by the oxidant and now exhibits a positive charge. In contrast to this general definition, Oxidation in terms of high temperature corrosion refers to the reaction with oxygen as the oxidizer. Oxidation in this context is the most important high temperature corrosion process, as oxygen is a part of most commonly appearing atmospheres. It is also the main topic of this thesis, investigating the high temperature stability of AlCrN/ AlCrO multilayer coatings.

2.6.1 Oxidation kinetics

Depending on the temperature, material, and other parameters, oxidation can show different characteristic reaction rates. Common examples are linear, parabolic and logarithmic mass increase, as well as linear mass loss. At high temperatures, parabolic mass gain prevails. As shown in fig. 2.9, the corrosion reaction decelerates over time but never stops. The formation of the oxide layer decreases the reaction rate due to the longer diffusion paths of the reactants. Mathematically, the law for parabolic oxidation can be formulated as:

$$(\frac{\Delta m}{A})^2 = k_p t \tag{2.10}$$

In this equation, Δm is the mass gain, A the total sample surface, and k_p the parabolic oxidation constant. High temperature oxidation requires inward diffusion of oxygen atoms through the oxide layer or outward diffusion of metal ions, whichever is faster (fig. 2.10). The thicker and the denser the oxide layer gets, the more the oxidation is slowed down [5].

The parabolic oxidation law (found by G. Tammann, 1920) can be directly derived from Fick's first law, as the increase in oxide layer thickness over time Δs is proportional to the flux of particles.

$$\frac{ds}{dt} = J = -D\frac{\Delta c}{s} \tag{2.11}$$

A special kind of high temperature oxidation is the parabolic breakaway oxidation. This oxidation shows the fundamental behaviour of a parabolic oxidation, but the formed oxide layer is much bulkier than the parent material, leading to crack formation or even flaking off. Due to this process, new surfaces are exposed to the oxidizing agent and the process starts anew. Linear mass gain as a result of high temperature corrosion can be observed for

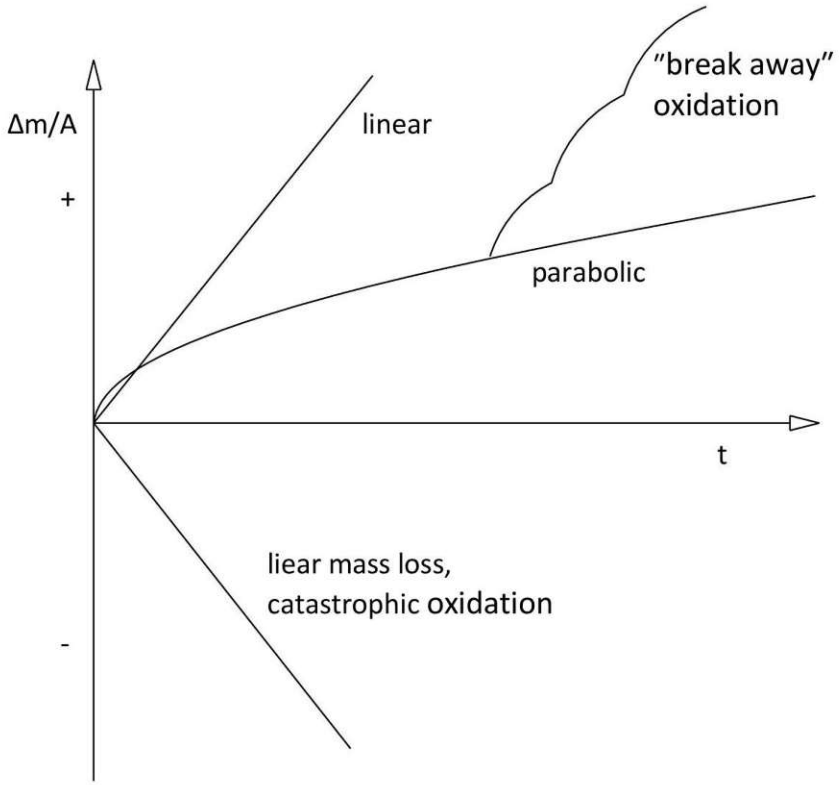

Figure 2.9: Compilation of various different forms of oxidation kinetics [5]

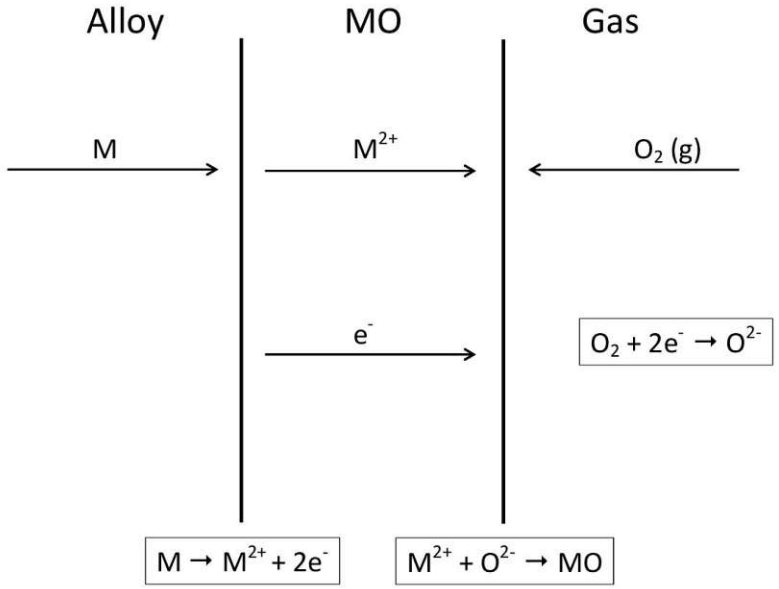

Figure 2.10: Diffusion of oxygen or metal ions lead to formation of the oxidation product at the interface [5]

e.g. Ta or Nb. These metals also have oxide layers with much lower density than the bulk material, which leads to even faster cracking of the oxide layer. This oxidation mechanism is known as breakaway oxidation. Among others, W and Mo show a linear mass loss from high temperature oxidation, this mechanism, commonly referred to as catastrophic oxidation, can only happen if the reaction products (the oxides) are fluids or volatile gases at the prevailing temperatures [5, 7, 19].

2.6.2 Oxidation resistance

Differing from traditional corrosion, where multiple ways of retarding or completely preventing corrosion are easily accessible, the nature of high temperature corrosion leads to very few possible strategies. As oxygen is a gas and high temperature oxidation is dominated by diffusion processes, the only way to slow down corrosion (apart from temperature-stable coatings, such as ceramics) is to decelerate diffusion. This can be accomplished by the formation of stable and very dense oxide layers on the material's surface. Elements like chromium, aluminium or silicon show high affinity to oxygen and form stable layers with low diffusivity. Therefore, it is often desirable to choose compounds with these elements or include at least low percentages to exploit their protective properties [5].

2.7 Characterisation techniques

2.7.1 Thermal analysis

As the mayor reason behind the execution of this master thesis is the thermal - and oxidation stability of coatings at elevated temperatures, obvious examination methods are the use of differential thermal analysis (DTA) and differential scanning calorimetry (DSC). These techniques provide data covering various thermal material properties such as phase stability, phase transformation or heat capacity. The findings are obtained by measuring the temperature (DTA) and heat flow (DSC) changes during exothermic and endothermic phase transformations. Multiple different experiments can be performed. For the purpose of this thesis an isothermal single-run testing procedure was selected to generate information concerning the oxidation stability of different coatings. Flaky powder samples were first heated in an inert He atmosphere to the testing temperature. After a short stabilisation time, the atmosphere was exchanged for synthetic air. Before cooldown the atmosphere was changed to He again. DSCs and DTAs can be equipped with scales to simultaneously measure mass and heat flow changes. A positive mass change during the experiment can be related to a reaction with an oxidising atmosphere, which leads to the incorporation of additional atoms into the structure, e.g. Oxygen, see fig. 2.11. A decreasing mass can be caused by decomposition with elimination of volatile reaction products, see fig. 2.12 [10, 20].

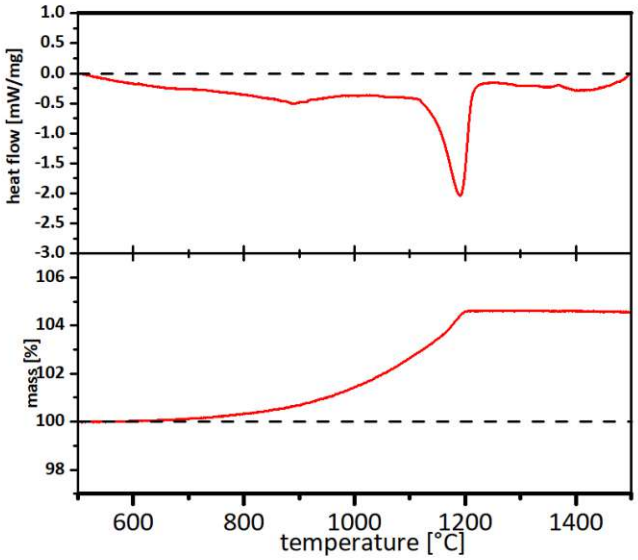

Figure 2.11: DSC and TGA analysis data for AlCrN/AlCrO multilayer coating with nitrogen to oxygen ratio of one in synthetic air; 80 bilayers, bilayer period around 30 nm

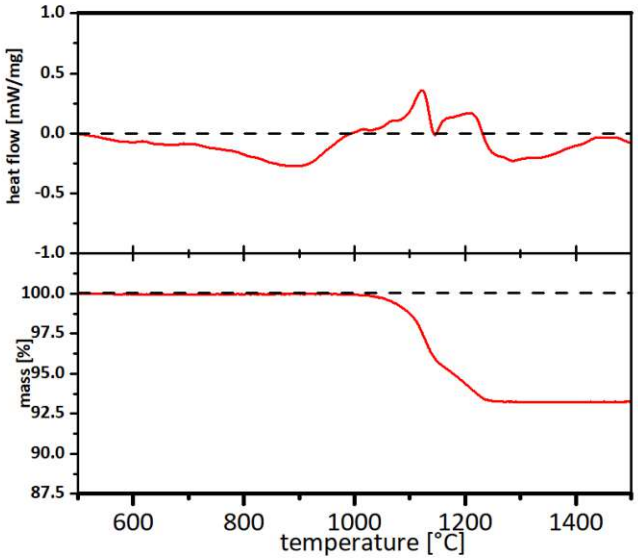

Figure 2.12: DSC and TGA analysis data for AlCrN/AlCrO multilayer coating with nitrogen to oxygen ratio of one in inert He atmosphere; 80 bilayers, bilayer period around 30 nm

2.7.2 Structural analysis

X-Ray Diffraction is a very common method for analysing crystal structures. It is based on the interaction of X-rays with atoms in a crystal lattice. Lattice parameters are the same order of magnitude as the wavelength of X-Rays. Therefore, X-rays are diffracted when interacting with crystal lattices. Depending on the angle of incidence, the lattice orientation and the wavelength, either constructive or destructive interference occurs between the reflected rays of different layers. If the X-ray intensity is plotted over the incidence angle, peaks show the angles of constructive interferences. This information can be used to determine the lattice parameters of the measured crystal if the crystal structure is known. Bragg's law shows this relation. (fig. 2.13) In Bragg's law, λ represents the wavelength of incoming light, n is a natural number to illustrate that only integral multiples of the wavelength lead to constructive interference. The distance between the atomic layers in the crystal is represented by d and θ stands for the angle of incidence.

$$n\lambda = 2dsin(\theta) \tag{2.12}$$

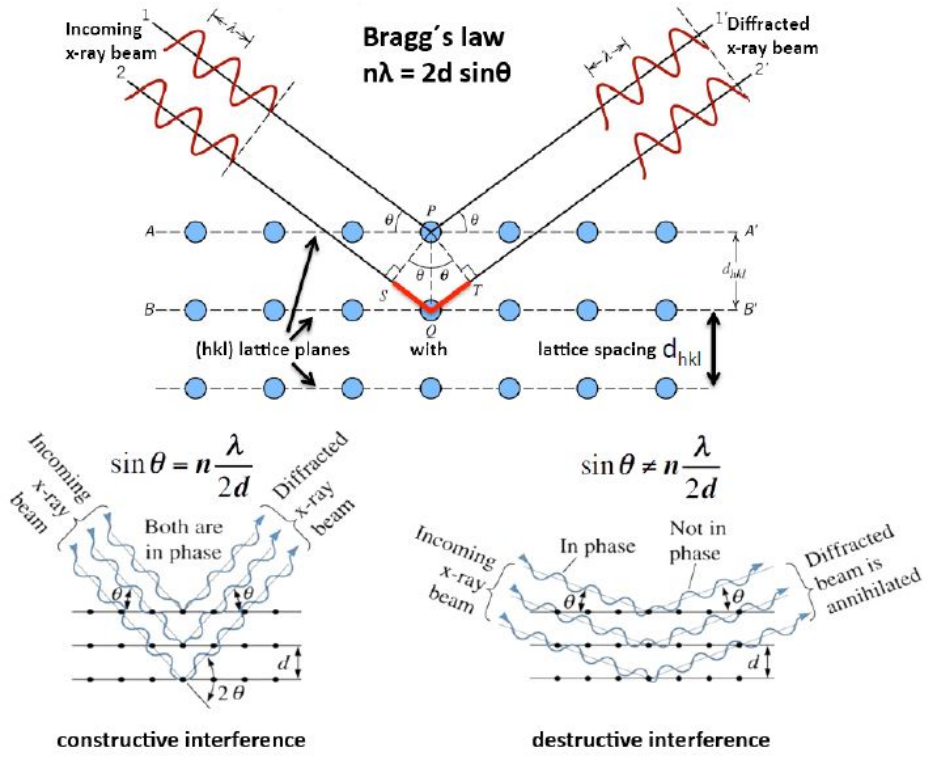

Figure 2.13: Bragg's law and the simplified interaction between crystal latices and X-Rays that can be used for its derivation [8]

For samples with known contents, the atomic composition ratios can be derived from the peak intensities with reasonable accuracy. XRD-analyses in this thesis were carried out using the $Cu_{K\ alpha}$ line with wavelength approximately 0.154 nm as a monochromatic X-ray source [7, 10].

2.7.3 Nanoindentation

Mechanical properties such as hardness and elastic modulus are important characteristics of thin film tool coatings. Due to the low film thickness, it is not possible to use Brinell or Vickers tests, which are standard hardness tests for bulk materials. The hardness of thin film coatings therefore has to be derived by nanoindentation, a measurement method using very small loads to penetrate the sample surface with a defined Berkovich indenter. Force and indentation depth are recorded simultaneously, resulting in a load-displacement curve as shown in fig. 2.14 [7].

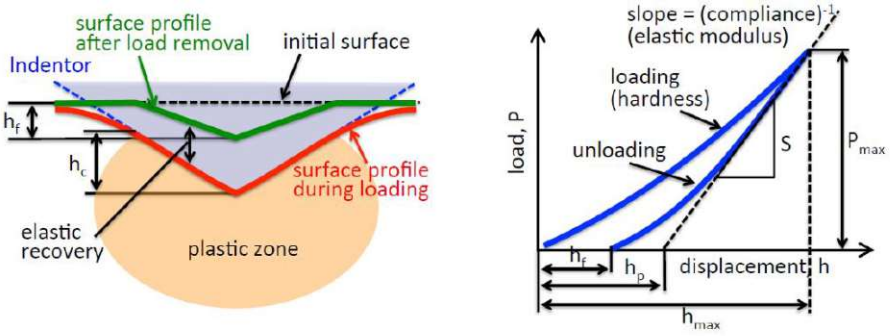

Figure 2.14: Material response to indentation (schematic) and load-displacement curve as obtained by nanoindentation [9]

Fig. 2.14 additionally shows the schematic response of a material undergoing a Nanoindentation test: during the loading process, elastic and plastic deformation are obtained. When the force is removed, the elastic deformation reverts to the undeformed state, while the plastic deformation remains. To exclude substrate influences, it is important for Nanoindentation measurements of thin film coatings that the indentation depth should not exceed 10% of the total film thickness.

2.7.4 Scanning Electron Microscopy

Scanning Electron Microscopy(SEM)is a characterisation technique where electron bombardment is used instead of visible light or other electromagnetic waves to obtain information. In particular, due to the low wavelength of electrons (which show particle - and electromagnetic wave properties simultaneously), it is possible to achieve much higher magnifications than with visible light, as the maximum resolution is dependent on the radiation wavelength. Scanning electron microscopes require a high vacuum to avoid collisions between electrons and air molecules. There are different approaches to generate the required electrons, possibly the most descriptive consists of a tungsten-Filament that is heated to elevated temperatures and supplied with a high voltage, the acceleration voltage. Tungsten is used because of its high melting point and low vapour pressure, so that the filament can be heated to temperatures which allow electron emission. Other methods of electron generation include lanthanum hexaboride (LaB_6) cathodes, which are used instead of tungsten in the same installation, or field emission guns (FEG) using different mechanisms. Independent from the used mechanism, the generated electron beams are then accelerated by the applied voltage and focused with lenses to a spot diameter in between approximately 0.5 and 5 nm. The beam is screened (directed by electromagnetic lenses)over the sample surface. The bombardment with electrons leads to electric charging of the sample if the sample is not conductive, which leads to bad imaging results. Therefore, non-conductive samples normally are sputtered with a very

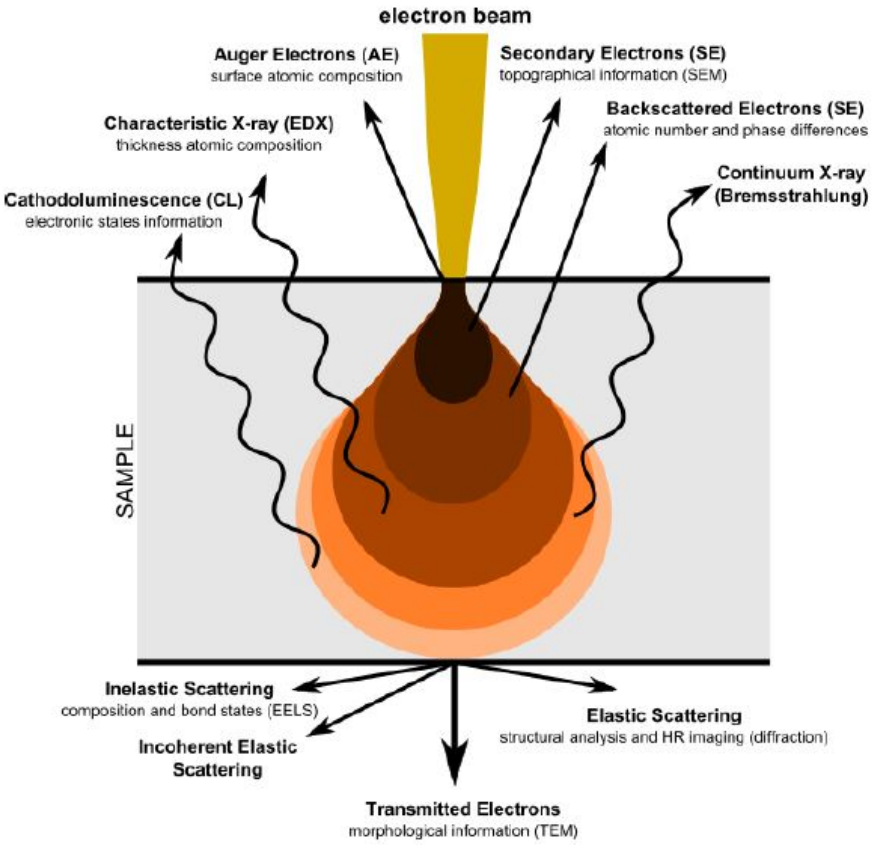

Figure 2.15: Results of the interaction between electron beam and sample [10]

thin, conductive layer of e.g. gold-palladium. This was also used for the samples examined in this thesis. upon incidence on the sample, multiple different interactions between electrons and the sample material can occur, leading to various different emissions that can be measured and used to characterize the sample, 2.15 [21].

Secondary electrons (SE) are electrons originating from the surface near sample regions and can therefore be used for topographic imaging, fig. 2.16. Backscattered electrons are reflected at the sample surface and contain additional information about the sample material. Electrons knocked out of their orbits by irradiating electrons emit characteristic X-ray radiation which can be used to determine the atomic composition of the sample or rather small sample volumes near the sample surface. This investigation method is called Energy Dispersive X-ray Spectroscopy or EDX [21].

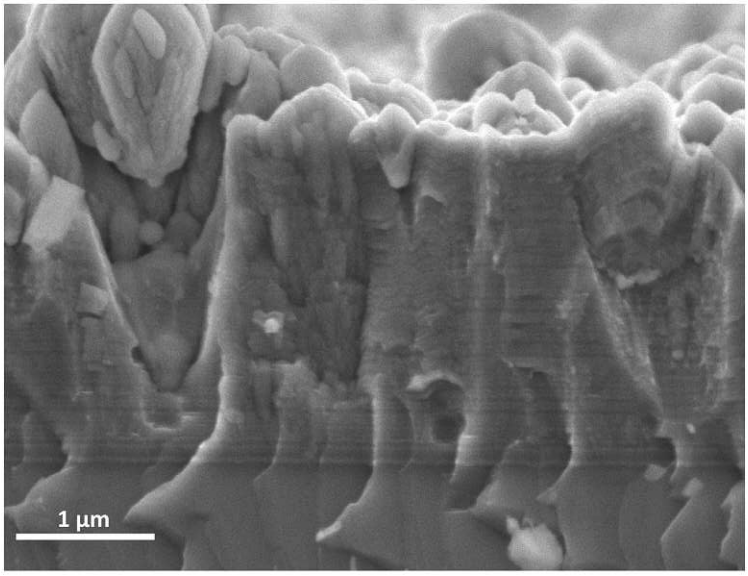

Figure 2.16: SEM-image of the cross-section of the sample with AlCrN/AlCrO ratio 1:2

Chapter 3

Experiments and results

Cutting tool coatings have been state of the art for years, with multiple different coating substances being used for varying applications. The main goals of these coatings are to enhance the mechanical properties, such as wear resistance or hardness, in combination with allowing for the use at higher operating temperature. This is especially important, because the ability to withstand higher temperatures under adverse conditions in ,e.g. oxidising atmospheres, significantly increases the productivity of cutting tool applications by reducing the dead time or cool-down periods. It is, in fact, one of the premier goals of continuous research on cutting tool coatings. Systems showing promising results in both mechanical properties and thermal stability include the aluminium-chromium based nitride and oxide configurations. As stated previously in sec.3.1, the crystallographic structure and with it the mechanical properties are very much dependent on the aluminium content of these coating systems, increasing with higher aluminium content up to the point where structural changes lead to the formation of phases with worse overall performance. This is mainly caused by the excellent properties of aluminium oxide, which unfortunately can up to now not be produced by means of PVD. Therefore, it is necessary to utilize the stabilizing effect chromium exerts on the formation of corundum-type compounds. In regard to the later applicability of the developed coatings, especially tests concerning the oxidation resistance and not only the thermal stability in a vacuum or inert gas atmospheres are invaluable. The behaviour of coatings in oxidising atmospheres at elevated temperatures fundamentally deviates from the reactions in inert atmospheres and plainly shows if newly developed coatings can really withstand higher operational temperatures at realistic applications or at least increase the lifetime of state of the art tools at common operating temperatures. For the purpose of this thesis, 5 different coatings with AlCrN/ AlCrO multilayer structure were deposited and tested to identify the thermal stability and oxidation resistance at elevated temperatures in comparison to each other. The PVD-coatings were all generated using an Oerlikon Balzers Innova batch-type cathodic arc evaporation system. The powder metallurgically (PM) prepared targets ($Al_{0.7}Cr_{0.3}$) were purchased from Plansee Composite Materials GmbH. Prior

Table 3.1: Deposition parameters for the sample production [10]

layer type	**arc current** (A)	**gas flow rate** (sccm)	**pressure** (Pa)
AlCrN	150	1100	3.6
AlCrO	180	1000	2.6

to the deposition process, the substrates (low alloy steel foil, silicon wafers, corundum and polycrystalline Al_2O_3 substrates) were cleaned with ethanol and mounted on a two-fold rotation carousel. After heating for 30 minutes to the deposition Temperature of $500°C$, an Ar ion etching step was carried out for 30 minutes. This procedure removes oxides and eventual residues from the substrate surfaces and thereby improves the adhesion between coating and substrate. The Multilayer architecture was achieved by alternating operation of two of the four active targets. For the oxide layer, two targets were operated in an oxygen atmosphere, while the nitrogen layer was deposited by using the remaining two targets and operating in a nitrogen atmosphere. The layer thickness was controlled by adjusting the operation time of the two target pairs. Detailed information concerning the parameters used or deposition can be taken from table 3.1 [10].

3.1 Structural properties

The scope of this thesis is the examination of the high temperature oxidation stability of AlCrN/ AlCrO multilayer coatings. To be able to give adequate explanations on the occurring reactions and mechanisms, it is necessary to first provide a quick overview concerning the composition and structure of the reviewed coating system.

3.1.1 AlCrN system

Ternary $Al_xCr_{1-x}N$ coating systems have been investigated for cutting tool applications recently. AlCrN coatings offer good mechanical properties, excellent wear resistance and show excellent tool life [22]. A major advantage over similar systems, such as TiAlN or AlTiN coatings, is the higher oxidation stability [22]. Studies [23–25] show that oxidation stability increases with higher aluminium content. The desired metastable fcc phase is limited by a maximum Al content of x = 0.7. Higher aluminium contents favour the formation of the hexagonal wurtzite-type structure [24, 25]. The superior oxidation resistance is caused by the formation of stable Al_2O_3 and Cr_2O_3 layers, which exhibit high oxidation resistance as stated in chapter 3.5 [10].

3.1.2 AlCrO system

AlCrO coatings exhibit even higher oxidation resistance and thermal stability than AlCrN coatings. This should not surprise, as CVD-generated Al_2O_3 coatings are known to show excellent mechanical properties and chemical resistance. The fabrication of corundum-type Al_2O_3 coatings via PVD is currently topic of extensive research, but could not be achieved yet. Therefore, AlCrO systems are used as a substitute. In this system, Cr_2O_3 stabilizes the formation of the desired corundum-type structure [26]. Again, the aluminium content has a big influence on the structure of the coating. High aluminium content is reported [27] to promote the formation of (metastable) fcc-type Al_2O_3 instead of the desired hexagonal corundum-type structure [10]. One drawback of AlCrO coatings produced by arc evaporation is the higher macroparticle defect density in comparison to AlCrN coatings. This can mainly be attributed to the higher number of droplet inclusions in AlCrO coatings. The defects serve as fast diffusion pathways and therefore have a negative effect on the oxidation resistance of AlCrO coatings.

3.1.3 Multilayer coatings

A well established method to improve the performance of thin film coatings is the application of multilayer arrangements. Depending on the layer thickness, multilayer architectures can accomplish different goals, reaching from the simple combination of two different materials

to enhance the coating properties and reap benefits of both materials to epitaxial growth stabilisation of structures that would not normally be stable for the used compounds. The latter requires very thin layers of very few nm [28]. Generally, multilayer composition has influences on the grain size and boundaries as well as on the dislocation and deformation behaviour, resulting in modified mechanical properties [28, 29]. Studies on AlCrN/ AlCrO multilayer coatings have established that the hardness, as well as the indentation modulus of multilayer coatings, increase with the number of layers or with decreasing bilayer period, fig.3.1. With suitable deposition techniques, it is also possible to generate different interface types, here referred to as blurred, hybrid and distinct. Blurred interfaces are generated by allowing an overlap between the deposition of AlCrN and AlCrO layers, leading to a mixed composition with a gradual transition between the distinct layers. Distinct interfaces are generated by not allowing deposition overlap, leading to well-defined boundary surfaces. Finally, hybrid interfaces are achieved by the combination of the two described deposition methods. Here, the transition between the nitride and the oxide layer is blurred, while the interface between the oxide layer and the nitride layer is distinct. These changes also have significant influences on the mechanical properties of multilayer coatings (fig.3.1) [10].

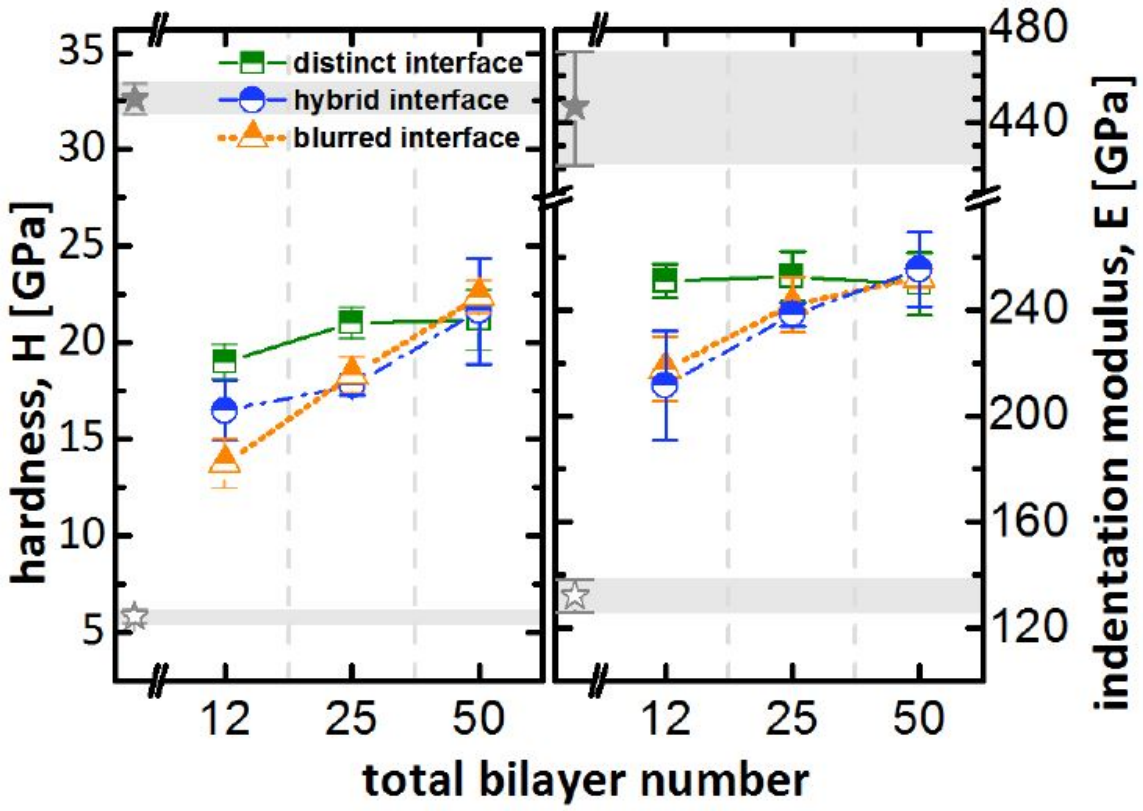

Figure 3.1: dependency of hardness and indentation modulus on the number of layers and the chosen interface type [10]

3.2 Coating composition

As stated in the previous section, multilayer arrangements of AlCrN and AlCrO were investigated. The two different components were deposited in alternating layers, which can be combined in pairs to a sequence of 80 identical AlCrN/ AlCrO bilayers. The number of 80 bilayer periods was chosen because prior investigations (sec.3.1.3 [10]), showcased improvement of mechanical properties with increasing number of layers. To identify the dependency of the oxidation resistance from the nitrogen content, 5 different coating compositions were elected, ranging from a AlCrN to AlCrO ratio of 1:4 to a ratio of 4:1. The overall coating thickness is in between 2.2 and 3.1 μm, while the average bilayer period is around 30 nm. The exact bilayer periods were derived by measurements with a FEI Quanta 200 Field Emission Gun Scanning Electron Microscope (FEG SEM) with an Energy Dispersive X-Ray Spectroscopy (EDS) detector attached. For this investigation, samples deposited on polycrystalline Al_2O_3 substrates were cleanly broken in half and the cross-section was examined (fig.3.3). The following table (tab.3.2) shows the chosen coating compositions and their respective average bilayer thickness, while fig.3.2 shows the measured average bilayer period with its standard

deviation compared to the estimated bilayer period derived from the total coating thickness. The fig.3.4 shows the composition of the 5 different coatings measured by XRD from the powdery samples later used for DSC testing.

Table 3.2: Coating compositions and their bilayer periods

sample	**N:O ratio (at%)**	**bilayer period** (nm)
AlCrN/O 4:1	4:1	35.47
AlCrN/O 2:1	2:1	35.44
AlCrN/O 1:1	1:1	35.38
AlCrN/O 1:2	1:2	28.56
AlCrN/O 1:4	1:4	32.84

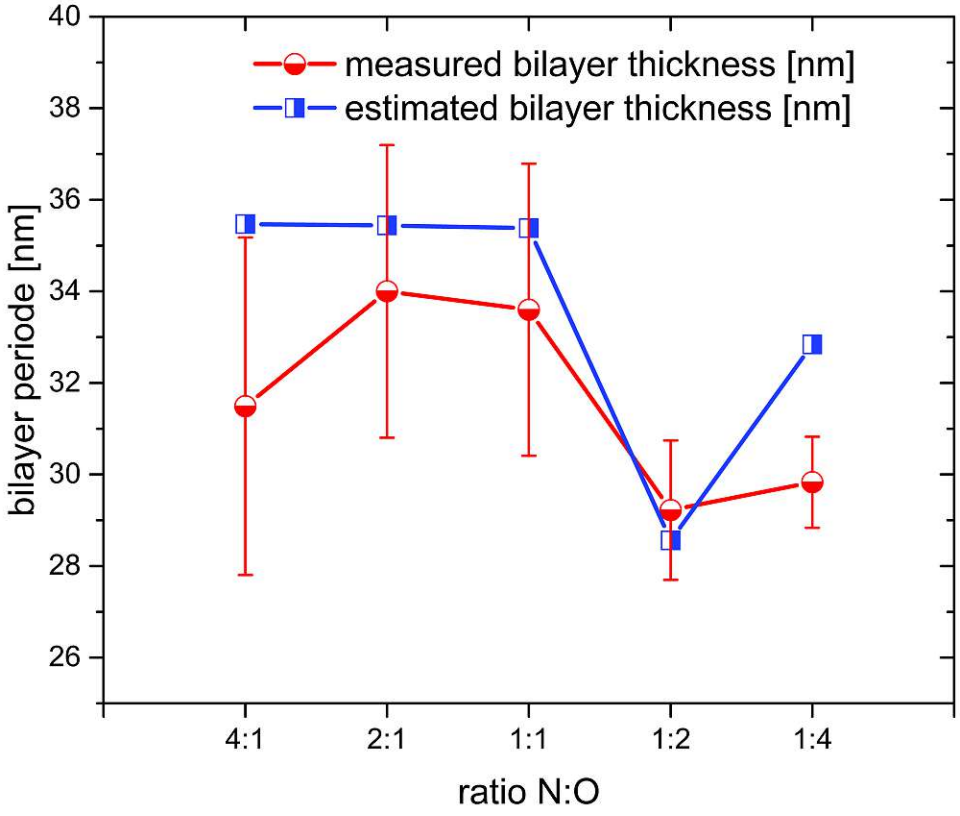

Figure 3.2: Measured average bilayer period with standard deviation in comparison to the estimated bilayer period derived from total coating thickness

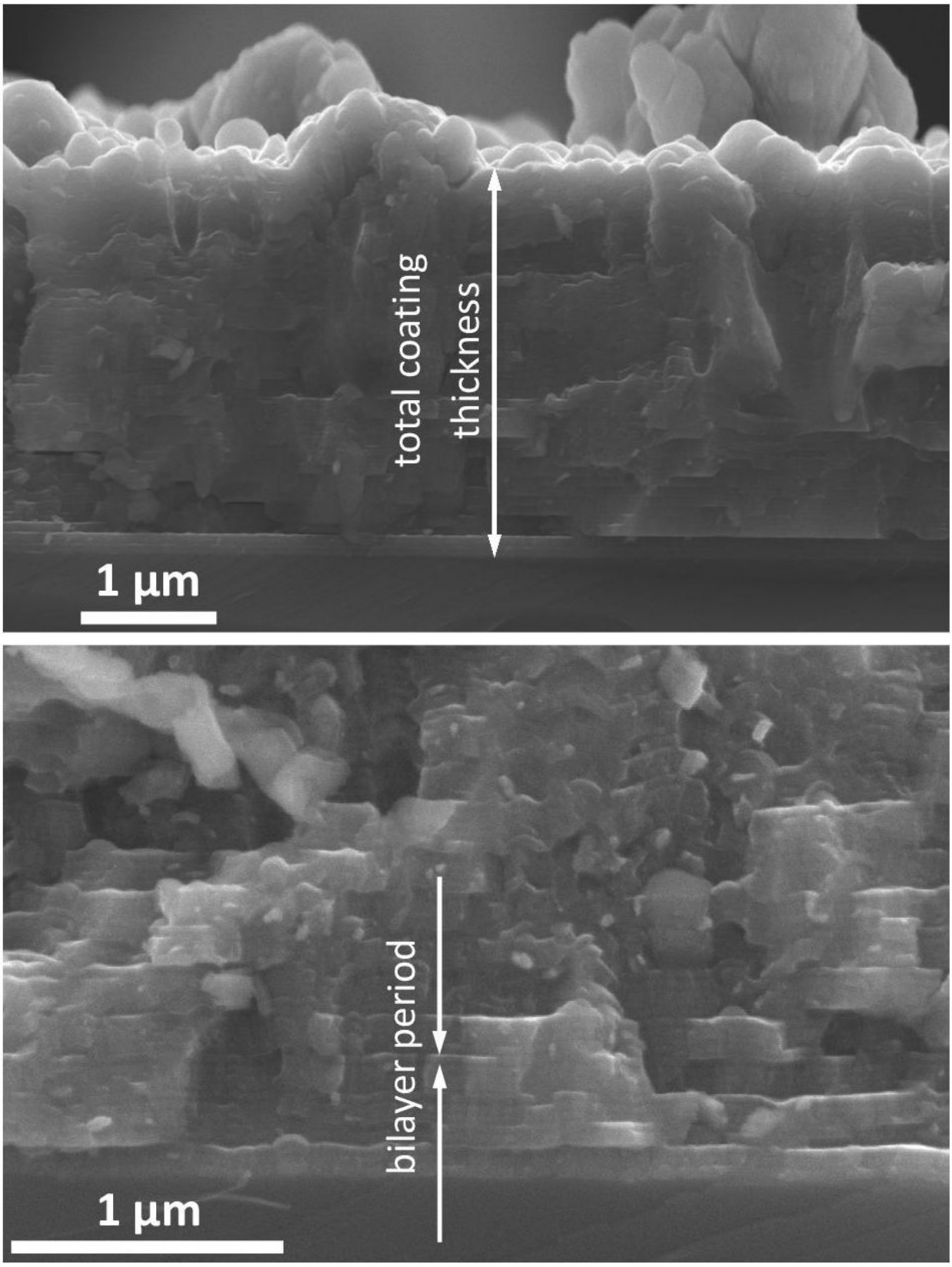

Figure 3.3: SEM-images showing the measurement of total coating thickness (top) and bilayer period (bottom)

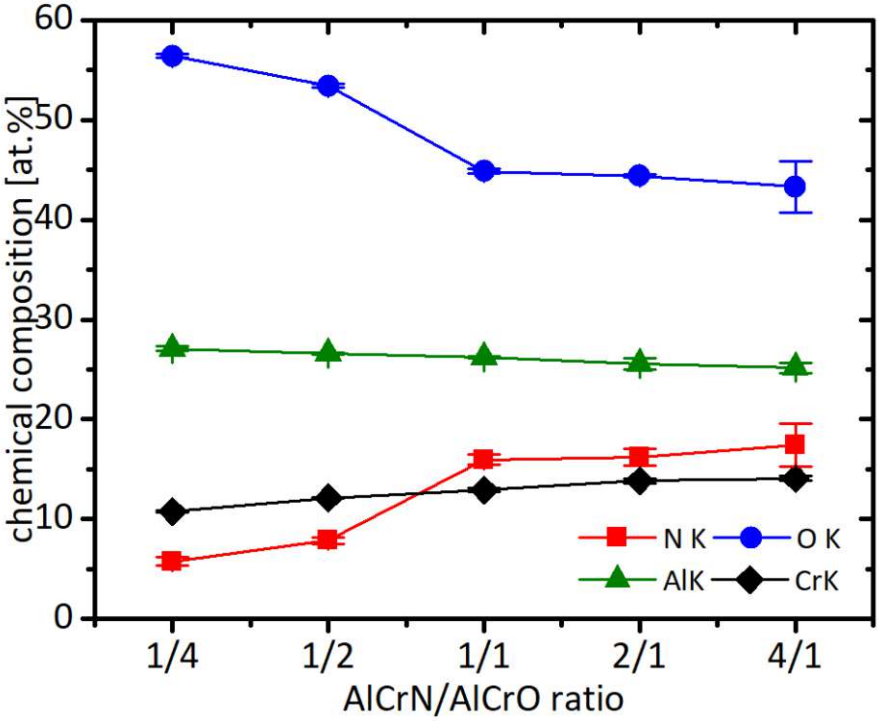

Figure 3.4: Composition of the investigated coatings in atomic percent, as derived by XRD from the ground as deposited state samples

3.3 Mechanical properties

The mechanical properties of the investigated coatings are, just as the thermal stability, very important parameters to decide if AlCrN/ AlCrO multilayer coatings show convincingly better performance than conventional coating systems. As stated in section 2.7.3, the dimension of thin film coatings does not allow for most common material tests, which is why nanoindentation was chosen to quantify the hardness and indentation modulus of the coatings. Fig.3.5 shows the derived mechanical properties depending on the chemical composition, thus the nitrogen to oxygen ratio.

Interestingly, no linear correlation seems to exist between mechanical properties and nitrogen content. Quite on the contrary, the determined results show a global maximum for the coating with N:O ratio 1:1 of approximately 23 GPa hardness and 275 GPa indentation modulus, as well as a local maximum for the 4:1 ratio coating, exhibiting almost the same mechanical properties as the 1:1 ratio coating. The coatings with ratios 1:2 and 2:1 show similar results in the range of $17 - 18$ GPa hardness and 240 GPa indentation modulus. Finally, the coating with N:O ratio 1:4 shows the by far worst performance with a hardness of around 14 GPa and indentation modulus of close to 180 GPa. All of the investigated coat-

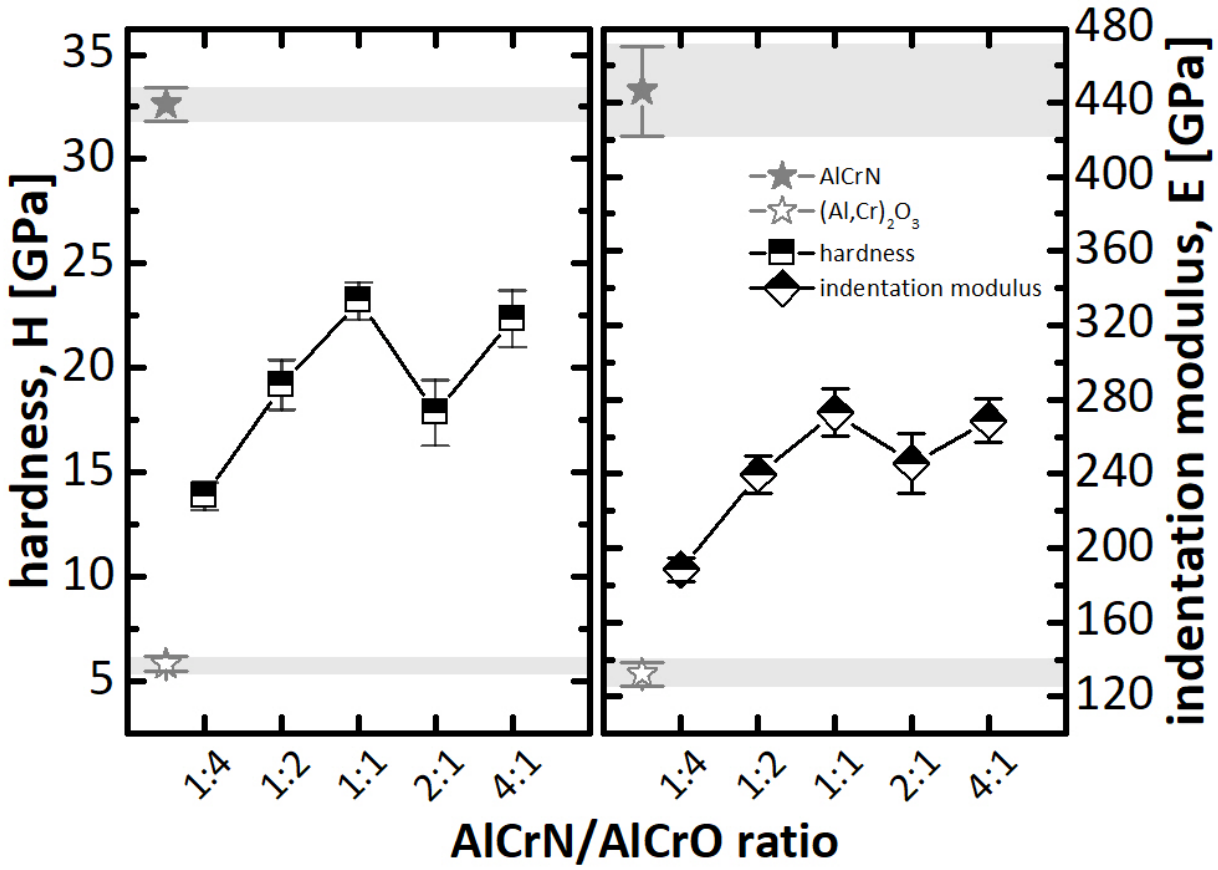

Figure 3.5: Hardness and indentation modulus of the different coatings; for comparison, the hardness and indentation modulus of monolithic AlCrN and $(Al,Cr)_2O_3$ coatings [10] are added into the diagram

ings show stabilities lower than monolithically grown AlCrN and higher than $(Al,Cr)_2O_3$ coatings. These comparative values were investigated during prior experiments [10] and are cited here to establish, that in terms of mechanical properties, no improvements whatsoever can be gained by the combination of AlCrN and AlCrO layers. Instead, the (hopefully) achievable amendments solely concern the thermals stability of tool coatings.

3.4 Thermal stability

Additionally to testing the oxidation resistance, also the thermal stability in inert gas atmospheres was tested. This experiment was carried out using a DSC-STA 449 F1 Jupiter, featuring a combination of differential scanning calorimetry (DSC) and thermal gravimetric analysis (TGA). Powdered coating materials were used in these measurements to exclude substrate influences on the results. The coatings were deposited on low alloy steel foil substrates, which were chemically removed by treatment with 35% hydrochloric acid at 70°C until no iron traces could be detected by XRD anymore. The detached coating flakes were then washed with acetone, which was in continuation evaporated before the remaining sample flakes could be ground to powder manually. The DSC-TGA measurements were carried out using a platin-iridium alloy crucible with an inlay of polycrystalline Al_2O_3. An identical crucible with inlay was used as reference sample. The samples were heated to 1500°C in helium atmosphere with a rate of 20 K/min. At 150°C an isothermal segment of 20 minutes duration was included to remove volatile contaminations [10].

The obtained information is plotted in fig.3.6. The mass loss and the measured heat flow are mapped against the temperature. Previous studies [RR] clarifying the occurring processes and crystallographic structures during the decomposition of AlCrN/ AlCrO multilayer coatings allow us to give detailed information about the processes that can be witnessed from DSC measurements. All samples show slow, continuous mass loss up to 1000°C which is accompanied by exothermic heat flow and can be attributed to recovery processes from deposition-induced defects. For the highest nitrogen content coating with N:O ration 4:1 we can see a pronounced mass loss starting at approximately 1050°C, showing endothermic heat flow activity. A second endothermic peak at approximately 1200°C can be observed as further, slower mass loss in the lower diagram. These peaks are caused by the dissociation of chromium-nitrogen bonds, where chromium-nitride first decomposes to Cr_2N and finally to Cr, always releasing N_2. This reaction is completed at approximately 1250°C and a total mass loss of little more than 9 %, from where on no further mass loss can be observed until the end. This means, that at 1250°C all nitrogen-chromium bonds have split and no nitrogen-chromium compounds remain. The same reaction can be observed for the coatings with N:O ratio 2:1 and 1:1 (yellow and red curve, respectively), with the sole difference, that the starting temperature is shifted to barely above 1100°C. The reaction ends at 1200°C again, with a total mass loss of around 6 %. The mass loss curves of this two coatings are almost superimposable, showing no notable difference in thermal stability between the two of them. However, the heat flow measurements show much less pronounced peaks for the N:O ratio 2:1 coating. The high oxygen content coatings with N:O ratios 1:2 and 1:4 (blue and green, respectively) also show similarities in their behaviour. Both coatings have a

distinct exothermic peak at 1100°C (N:O 1:4) or 1180°C (N:O 1:2) which can be attributed to the phase transformation from fcc and/or γ-Al_2O_3 to α-Al_2O_3 phases. They also both only exhibit one distinct endothermic peak that can be associated with the mass loss caused by Cr-N bond splitting. The total mass loss is higher for the 1:2 nitrogen to oxygen ratio coating, as can be expected from the previous results, but the starting temperature for the decomposition seems to be higher for the lower oxygen content coating. Generally speaking, the results indicate that the thermal stability of AlCrN/ AlCrO multilayer coatings derived by DSC analysis increases with higher oxygen content, which signifies that the AlCrO layers are acting - as intended - as diffusion barriers for the nitrogen in the powdery probe and retard the decomposition to Cr and N_2.

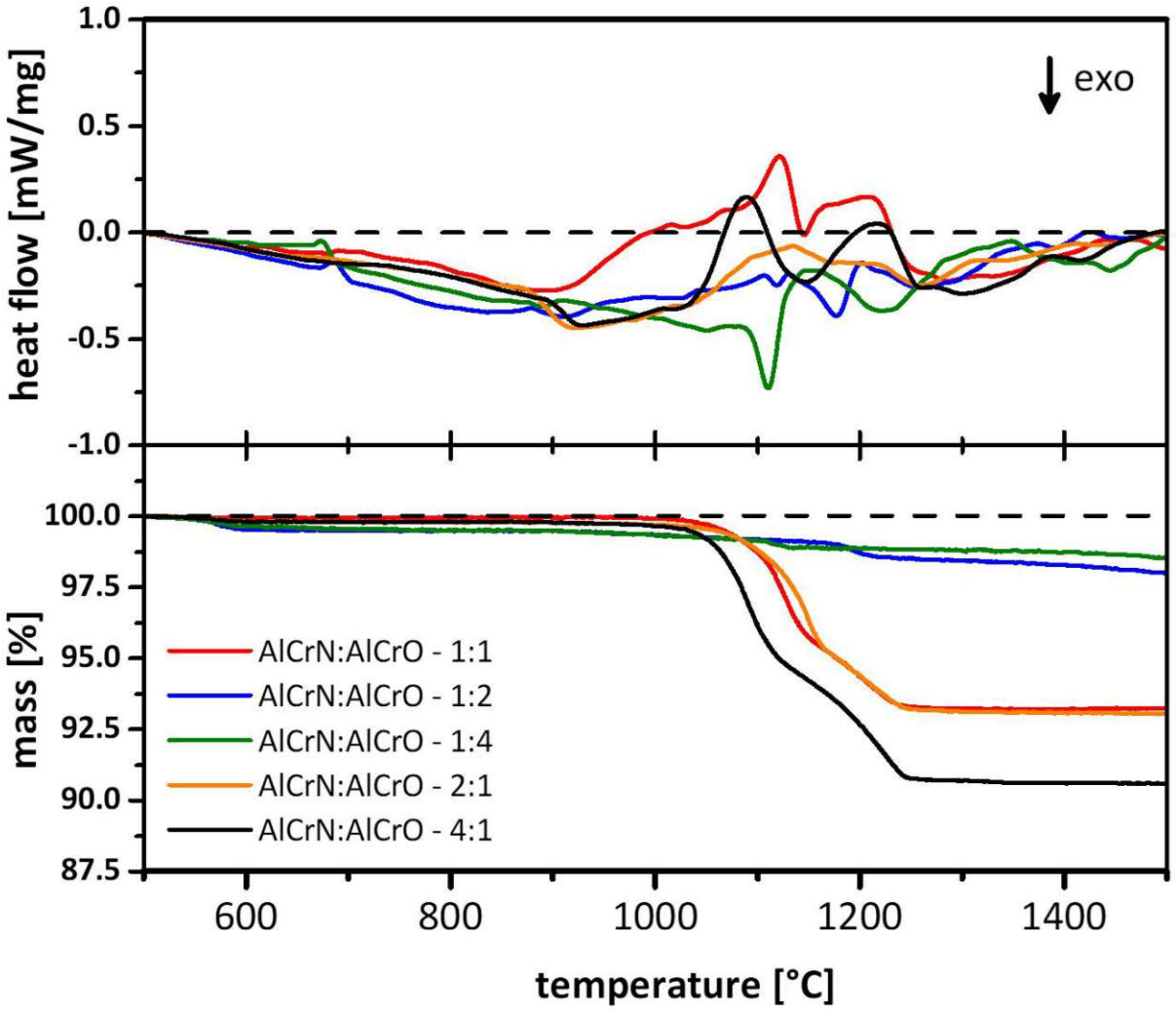

Figure 3.6: Heat flow and mass loss plotted against the temperature for all 5 coating compositions

3.5 Oxidation resistance

3.5.1 DSC-TGA analysis

Like for the thermal stability, the first step in testing the oxidation resistance of the coatings was to execute a combined DSC-TGA analysis. For this experiment, the same testing configuration (DSC-STA 449 F1 Jupiter, pulverized samples, Pt-Ir crucible, etc.) as in section 3.4 was used. The sample was heated to 1600°C with a rate of 10 K/min, and this time synthetic air was used instead of He as the atmosphere. At 150°C an isothermal segment of 20 minutes duration was included to remove volatile contaminations.

The obtained results are combined in fig.3.7. The mass loss and the measured heat flow are mapped against the temperature. All 5 samples show similar behaviour in this experiment. Beginning at 800°C, all samples start to gain mass due to oxidation processes. During this process, the coatings are deprived of nitrogen, as it is slowly exchanged for oxygen. This is continued until a stable plateau is reached, which happens between 1050°C and 1150°C for the high oxygen content coatings (N:O 1:4, green and 1:2, blue)and barely below 1200°C for the high nitrogen content coatings (N:O 1:1, 2:1, 4:1). Up to that point, the low nitrogen content coatings receive a mass increase of around 1 %, while the other coatings gain approximately 5 to 6 %. In the heat flow diagram, this reaction is represented by a single exothermic peak for all 5 coatings. The two lower nitrogen content coatings also lose mass after an initial mass increase. This loss may be explicable by the formation of volatile chromium oxides, which would mean that the mass gain due to oxidation is nearer 1,5 to 2 % for these coatings. Anyway, the high oxygen content coatings prove to be far less reactive than their high nitrogen content counterparts. The separation between the two groups is - just as it was for the thermal stability - between nitrogen to oxygen ratio 1:1 and 1:2. All coatings with higher nitrogen content show a generally high mass gain, while the two remaining low nitrogen content coatings seem to withstand these adverse conditions much better.

3.5.2 Long-term DSC-TGA analysis

Based on the results summarized in the previous section 3.5.1 and the mechanical testing data that can be found in section 3.3, one coating was selected for further oxidation resistance tests. As the oxidation stability is the primary scope of this thesis, only the two best coatings with N:O ratios 1:2 and 1:4 were considered for further investigation. Since the oxidation resistance of these two is almost identical, and the coating ratio 1:2 shows far better mechanical properties, it was finally selected for further testing. The additional tests were carried out to gather information concerning the long-term stability of the coating. These data were afterwards used to determine the testing parameters for yet another test series, now

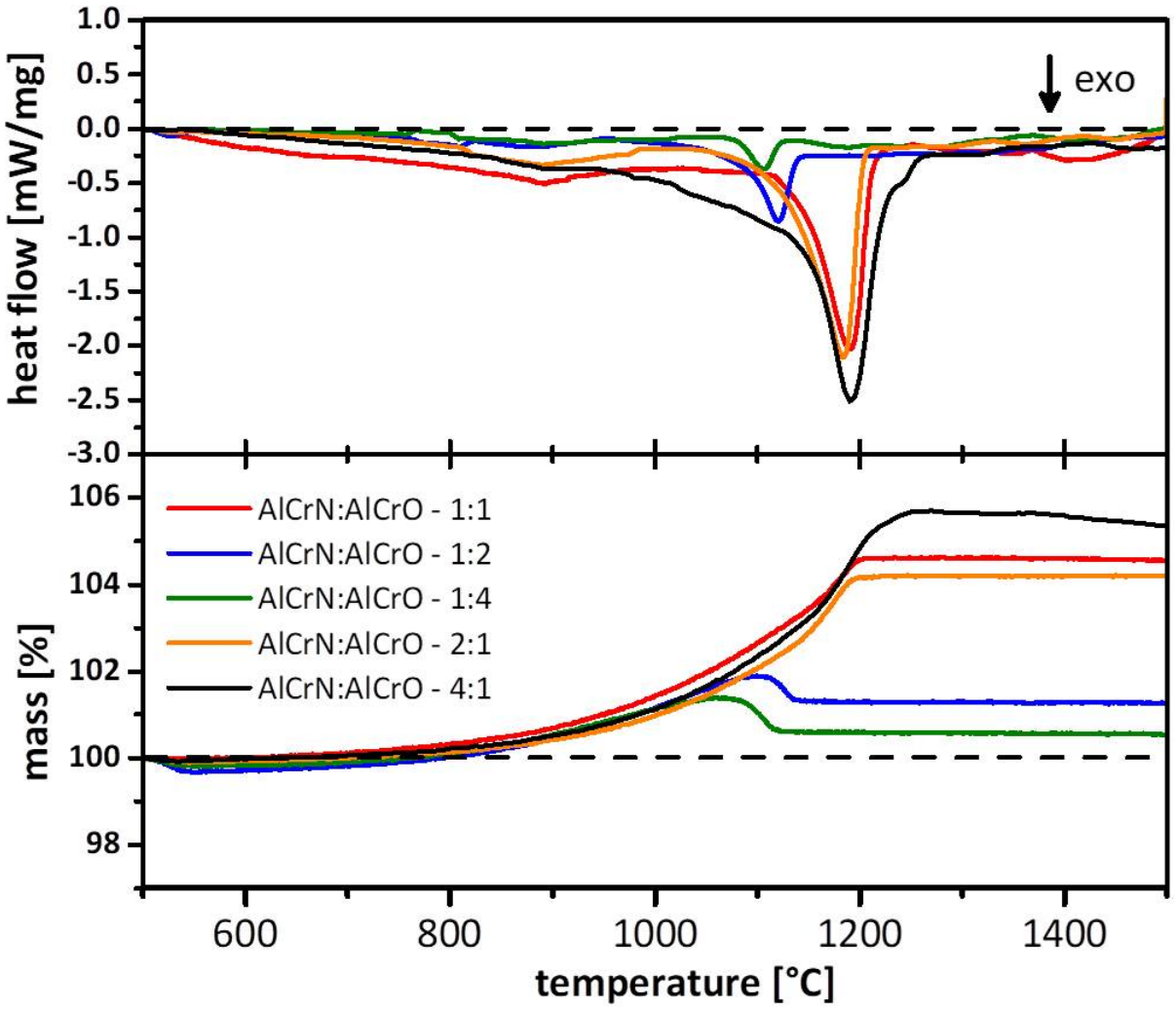

Figure 3.7: Heat flow and mass loss plotted against the temperature for all 5 coating compositions

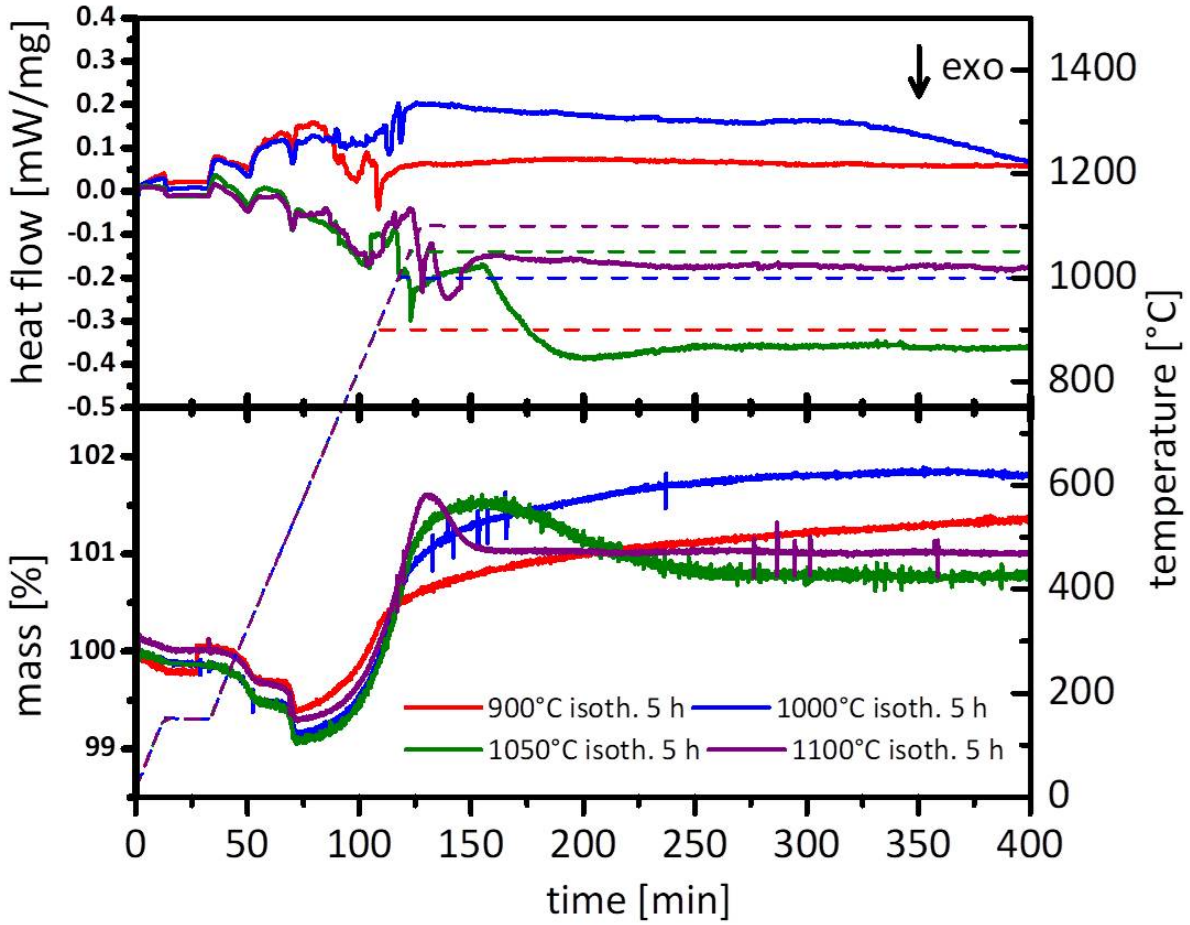

Figure 3.8: DSC results of the long-term oxidation tests with the N:O ratio 1:2 coating at different temperatures

featuring all 5 coatings, but this time in as deposited state. The long-term tests were, again, carried out using the DSC-STA 449 F1 Jupiter, with all the specifications already explained in detail in section 3.4. This time, however, the testing time was significantly increased to 5 h, while different maximum temperatures were chosen to find out which conditions the coating could at best endure in oxidising atmosphere for this time period. Obviously, the experiments were again executed with synthetic air for atmosphere, and temperatures of $900, 1000, 1050$ and $1100°C$ were elected for the test. The additional isothermal step at $150°C$ was once again included to expel volatile contaminations. The testing results are plotted in fig.3.8.

The diagram fig.3.8 shows the heat flow, mass gain, and temperature versus the testing time. The temperature profiles (dashed lines) show the different final temperatures as well as the isothermal step at 150°C. As can easily be deduced from the mass gain diagram, the coating oxidises faster when higher temperatures are applied. As a measure of oxidation stability, the time to reach the maximum mass gain was reviewed. While the coating never reaches a maximum during the testing period at 900°C, the maximum is hit rather quickly for higher temperatures like 1050 or even 1100°C. The measurement at 1000°C seems to exhibit a maximum shortly before the end of the testing period, after approximately 350 minutes. This led us to the conclusion, that the maximum tolerable temperature for a duration of 5 hours is close to 1000°C. Therefore the next test was carried out at that temperature.

3.5.3 Long-term furnace analysis

The experimental data of section 3.5.2 were used for further testing of all available coatings. The experiment was carried out using a high temperature furnace at 1000°C. The employed samples were deposited on mono-crystalline corundum substrate and used in the as deposited state. The goal of this testing procedure was to obtain performance data using parameters that were very close to the harsh conditions the coating would have to endure in real applications. The results of this process should allow us to evaluate the commonly used DSC-testing as a way to establish the oxidation resistance, as well as give insights into the maximum tolerable conditions if applied for tools. Therefore, the oxidation depth, meaning the thickness portion of the coating which was affected by high temperature corrosion, was of supreme interest for us.

Three specimens of each of the five coatings were heated in the oven. After 1 h, 10 h and 30 h, respectively, one of each coating type was taken out and cooled to room temperature. Now, the annealed samples plus one additional unheated sample for each coating were embedded in graphite containing plastic, polished to 1 μm abrasive grain size, sputtered with Au-Pd and the cross-section was examined using SEM. Additionally, EDX line scans were realized to determine the chemical composition of the cross-section.

The SEM-images show distinct differences between the oxidised and unharmed coating portions. This visual information was used to review the line scan results. The line scan results show the contents of nitrogen, oxygen, chromium and aluminium in the coating. The oxidized coating parts obviously exhibit higher oxygen and lower nitrogen content. The decomposition process is the same as for previous tests, the nitrogen gets expelled from the coating by the oxidizing oxygen. The scan results show a gradual depletion of oxygen over the coating thickness. This can be contributed partly to the diffusion gradients leading to the decomposition, and partly to the finite minimal spot size of the irradiating electron beam. All material stimulated by the electron beam emits characteristic x-rays. This leads to a

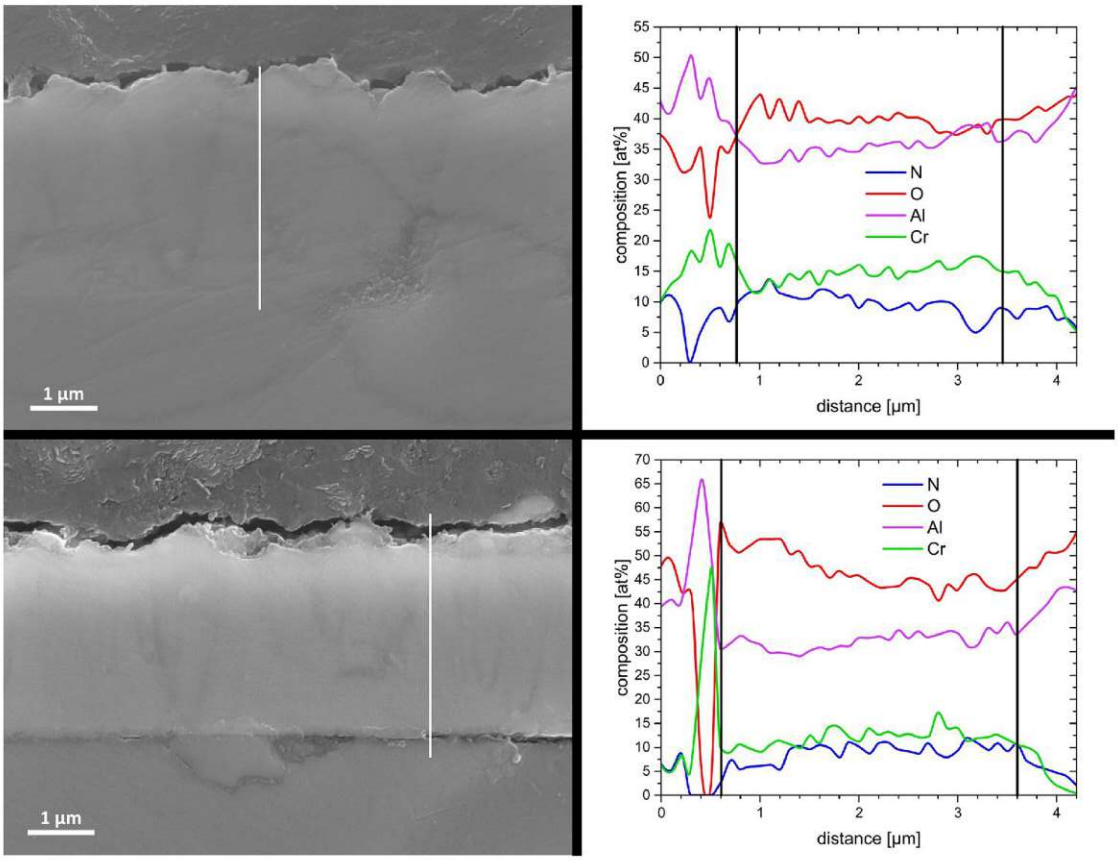

Figure 3.9: SEM-images and EDX line scan results for the N:O 1:2 coating; top: as deposited state; bottom: after 1 h of annealing at 1000°C; the white line specifies the line scan position; the two black lines in the diagram define the borders of the multilayer coating

gradually changing measurement result. For evaluation, the inflexion point of the gradient was elected to represent the oxidized thickness percentage of the coating. The following images fig.3.9 - fig.3.14 show some of the obtained cross section images and line scan data elected for further discussing the results. Fig.3.15 finally shows a compilation of all the obtained oxidation resistance data for all coatings. All of the cross sections and line scans not pictured in the following paragraph are attached in the appendix of this thesis.

Fig.3.9 shows the N:O ration 1:2 coating in as deposited state and after 1 h of annealing at 1000°C. In the line scan, the nitrogen content is represented by the blue line, while oxygen is represented by the red graph. The location of the line scan measurement is indicated by the white line in the SEM image. The two vertical black lines in the line scan diagram indicate the borders between multilayer coating and substrate or embedding material. When comparing the two line scans, it is apparent that the nitrogen content of the coating in as

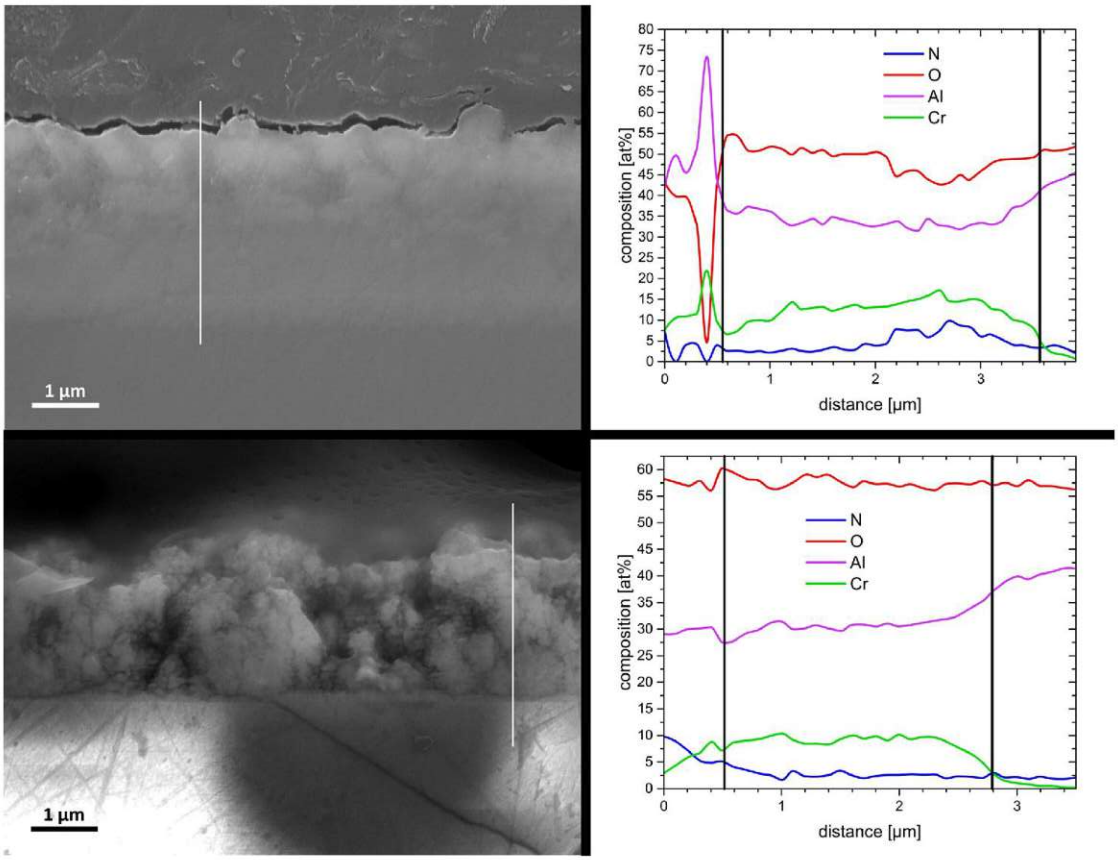

Figure 3.10: SEM-images and EDX line scan results for the N:O 1:2 coating; top: after 10 h of annealing at 1000°C; bottom: after 30 h of annealing at 1000°C; the white line specifies the line scan position; the two black lines in the diagram define the borders of the multilayer coating

deposited state does not change across the cross section. The annealed coating, on the other hand, shows a slightly decreased nitrogen content at the surface near coating portion. The coating with N:O ratio 1:2 was selected for the additional tests because of its remarkably high oxidation resistance in the DSC experiments. Therefore, if the DSC results are comparable to the results obtained by the more realistic approach of heating the full sample in as deposited state, we would expect high oxidation resistance at this test as well.

After further annealing, the sample with N:O content 1:2 suffers advancing decomposition. After 10 h, [fig.3.10, top) roughly half the coating has been affected by high temperature corrosion and exhibits significantly lower nitrogen content than in as deposited state. Also, the rising oxygen content is clearly visible. additionally, we can observe a slight decrease in chromium content. This is, as stated in sec.3.5.1, evidence for the formation of volatile

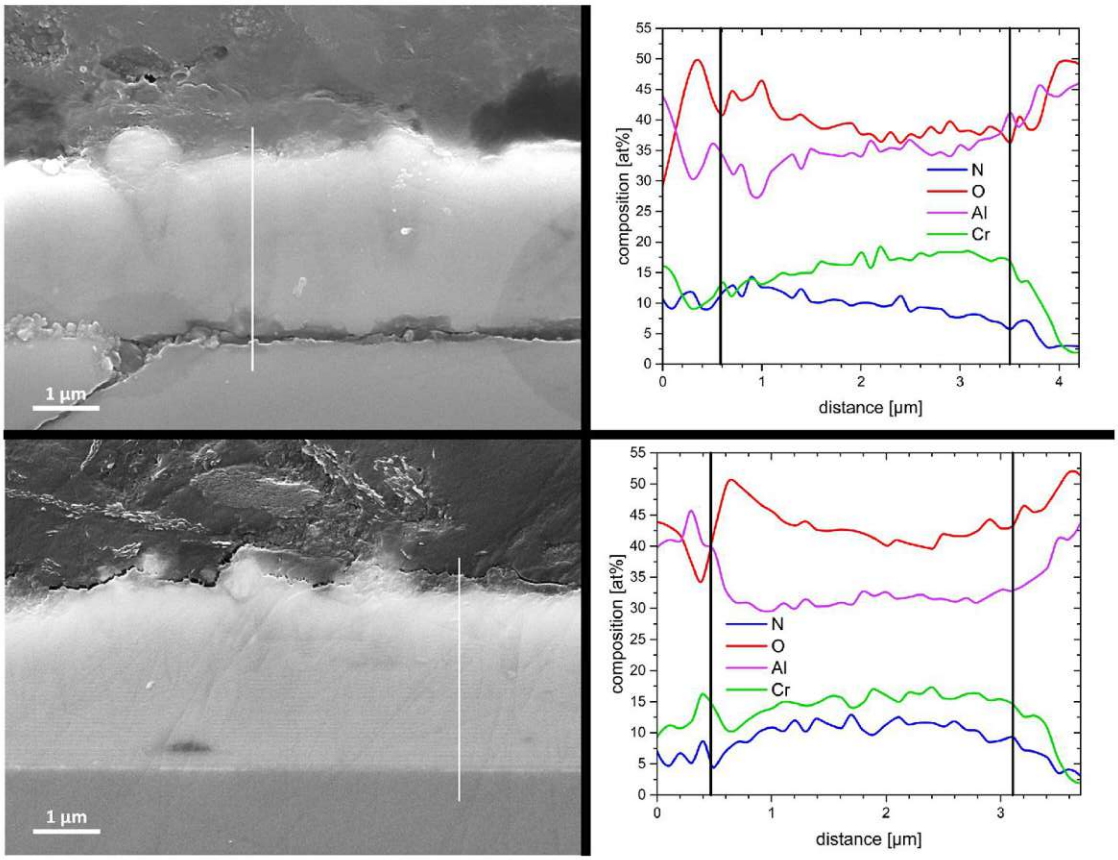

Figure 3.11: SEM-images and EDX line scan results for the N:O 2:1 coating; top: as deposited state; bottom: after 1 h of annealing at 1000°C; the white line specifies the line scan position; the two black lines in the diagram define the borders of the multilayer coating

chromium oxides at elevated temperatures. Finally, after 30 h of annealing, the coating is completely degraded and would provide no protective functionality whatsoever. We can observe multiple oxidation canals running straight from the coating surface down to the substrate. Also, the coating thickness has decreased in comparison to the 10 h annealed sample, further proof that volatile components are formed and expelled.

The coatings with N:O ratio 1:1 and 1:4 show far worse performance than the coating with ratio 1:2. This is, in case of the 1:1 ratio coating, an expected result, while it is quite surprising for the coating with ratio 1:4, as this configuration showed very promising oxidation resistance (in fact, better resistance than the 1.2 ratio coating) during the DSC tests. All the images and line scan data for the two coatings are attached in the appendix.

The expected result for the coating with N:O ratio 2:1, as pictured in fig.3.11 and fig.3.12,

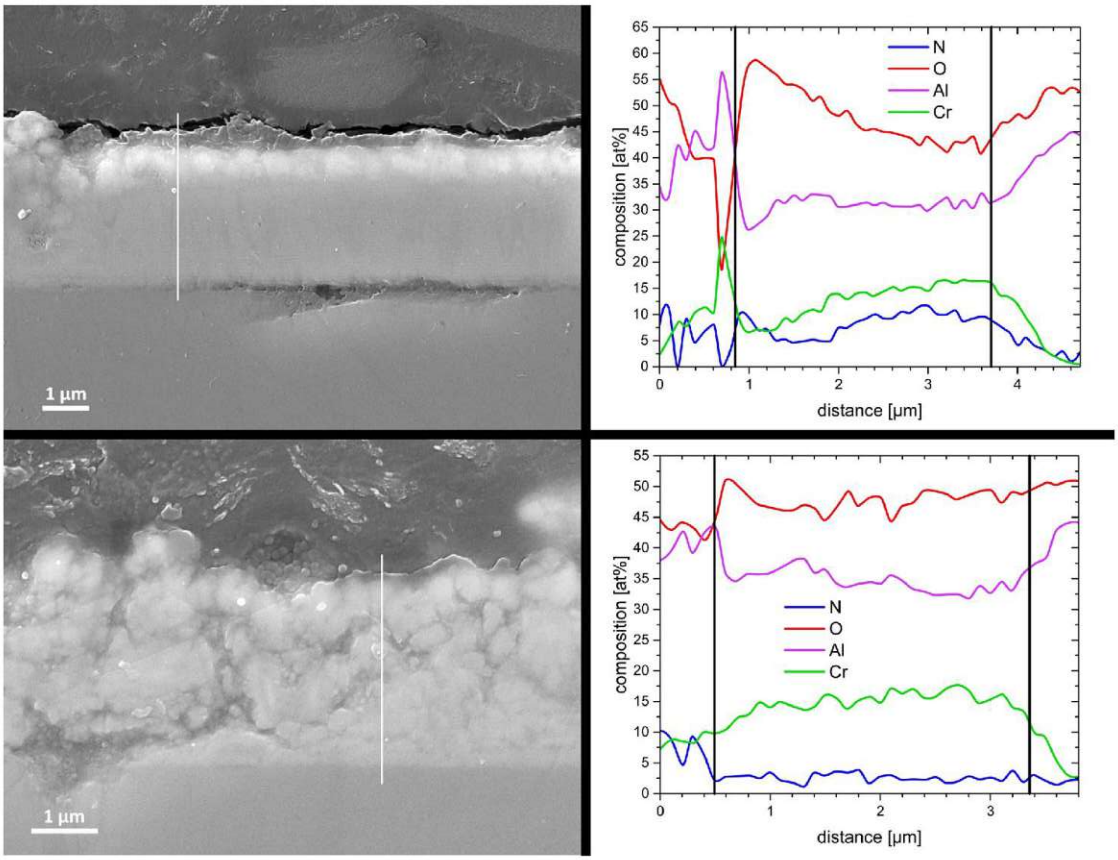

Figure 3.12: SEM-images and EDX line scan results for the N:O 2:1 coating; top: after 10 h of annealing at 1000°C; bottom: after 30 h of annealing at 1000°C; the white line specifies the line scan position; the two black lines in the diagram define the borders of the multilayer coating

would be a far worse performance than the previously examined coating with ratio 1:2 exhibits. As fig.3.11 shows, the results after 1 h annealing are not that different from the coating with ratio 1:2, with only slightly increased oxidation damage.

Fig.3.12 shows the same coating with ratio 2:1 after 10 h and 30 h of annealing. Interestingly, the oxidized coating portion after 10 h is significantly smaller than for the coating with ratio 1:2. After 30 h, this coating also has completely decomposed, however, the remaining structures seems to be more coherent than the remains of the coating with ratio 1:2.

The observed trend continues with the next coating, N:O ratio 4:1. While the oxidation resistance after 1 h seems to be slightly worse than for the coating with ratio 1:2 (fig.3.13), it by far exceeds the expectations on oxidation resistance after 10 h and 30 h (fig.3.14). Here we

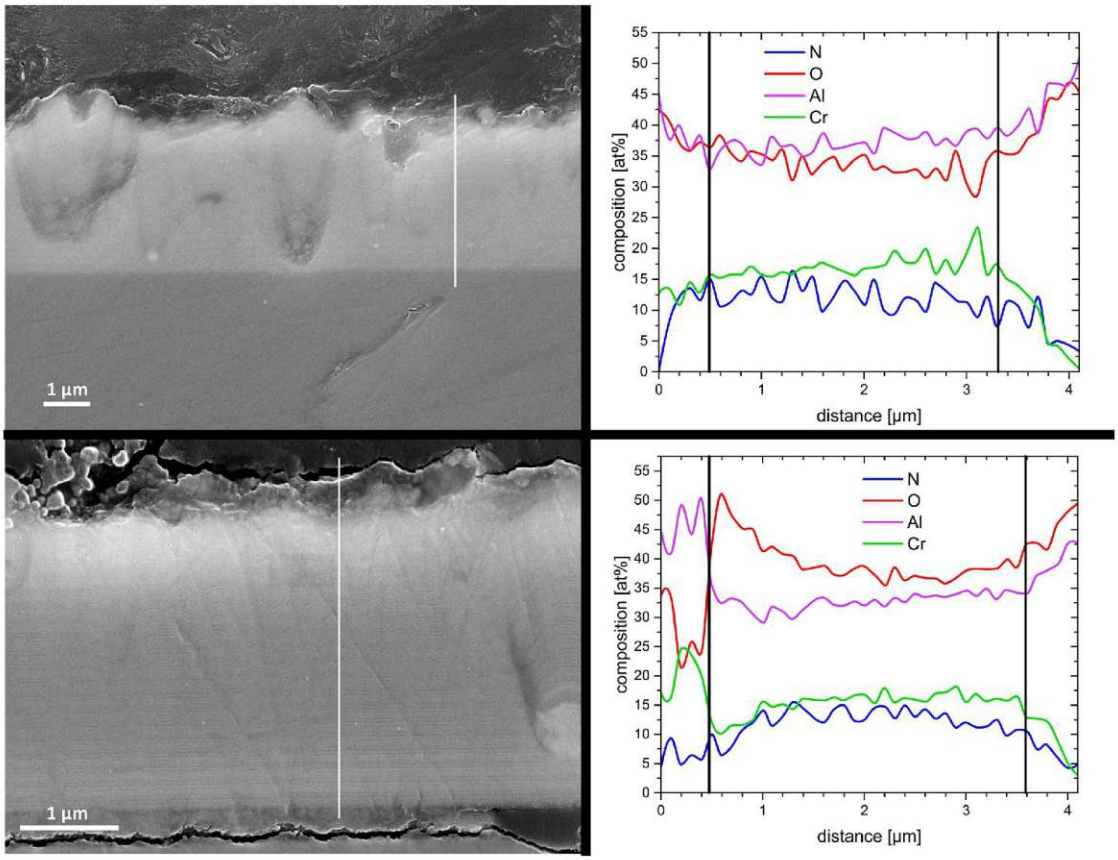

Figure 3.13: SEM-images and EDX line scan results for the N:O 4:1 coating; top: as deposited state; bottom: after 1 h of annealing at 1000°C; the white line specifies the line scan position; the two black lines in the diagram define the borders of the multilayer coating

can observe an even lower thickness percentage, in comparison to the 2:1 coating, is oxidized after 10 h. Additionally, this coating still has not completely decomposed after 30 h, around 20 % of the initial coating thickness remain untouched.

The following fig.3.15 shows a compilation of all the data concerning the oxidation depth that were obtained during the long-term furnace oxidation test. The three different exposure times are each represented by an individual curve, while the coating type is noted at the x-axis. From this diagram, we can deduce that there is no linear dependency between the oxidation resistance and the nitrogen content in the coating. However, we can remark that in general, higher nitrogen contents are very beneficial for the oxidation stability. Especially after longer exposure, when the differences between the coatings are getting more pronounced, it is obvious that the high nitrogen coatings outperform the other coatings quite distinctly. The coating exhibiting the highest oxidation resistance is the coating with N:O ratio 4:1,

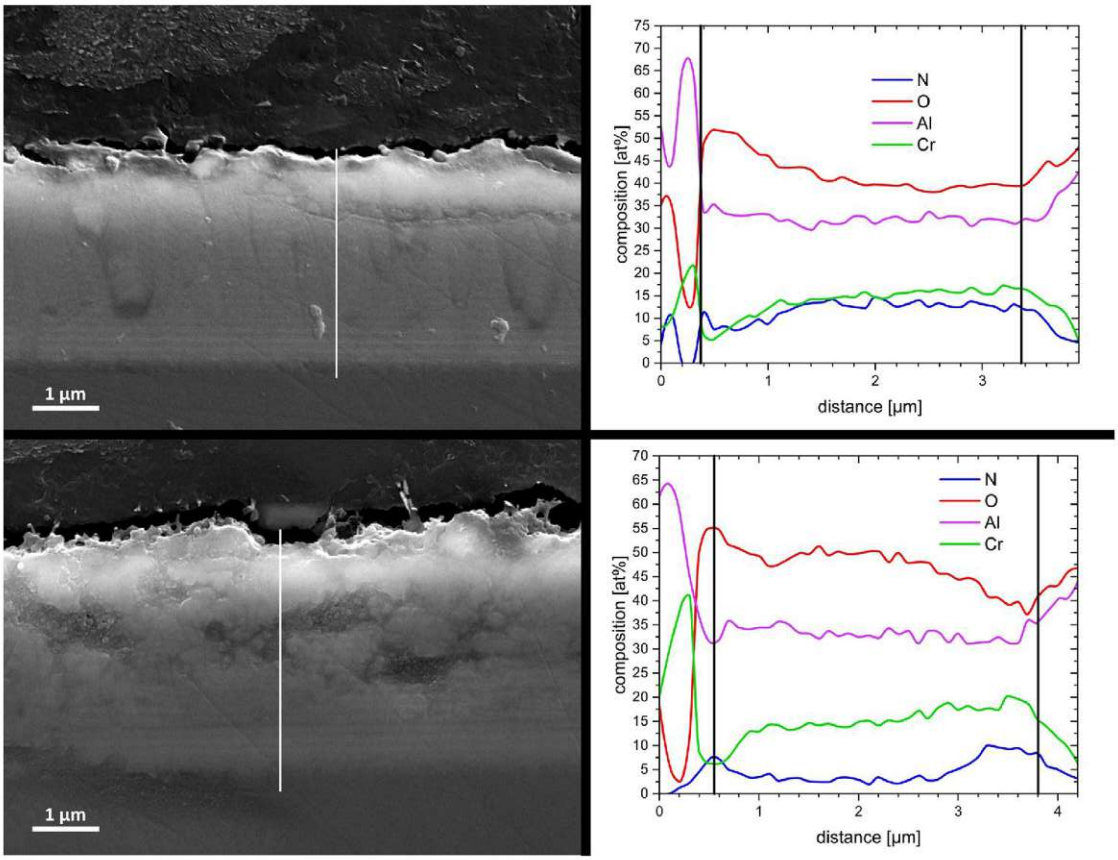

Figure 3.14: SEM-images and EDX line scan results for the N:O 4:1 coating; top: after 10 h of annealing at 1000°C; bottom: after 30 h of annealing at 1000°C; the white line specifies the line scan position; the two black lines in the diagram define the borders of the multilayer coating

which is not even completely decomposed after 30 h. On the other side of this spectrum, we have the coating with ratio 1:4, which is destroyed after just 1 h of exposure. The only coating breaking the trend to lower stability with lower nitrogen content is the coating with ratio 1:2, which shows far better results than the coating with ratio 1:4 and as well as the coating with ratio 1:1. However, apart from its superb results after 1 h of exposure, it is still worse than both of the high nitrogen content coatings in this test. This result precisely contradicts the results obtained earlier in sec. 3.5.1, where higher oxidation stability was observed for the high oxygen content coatings.

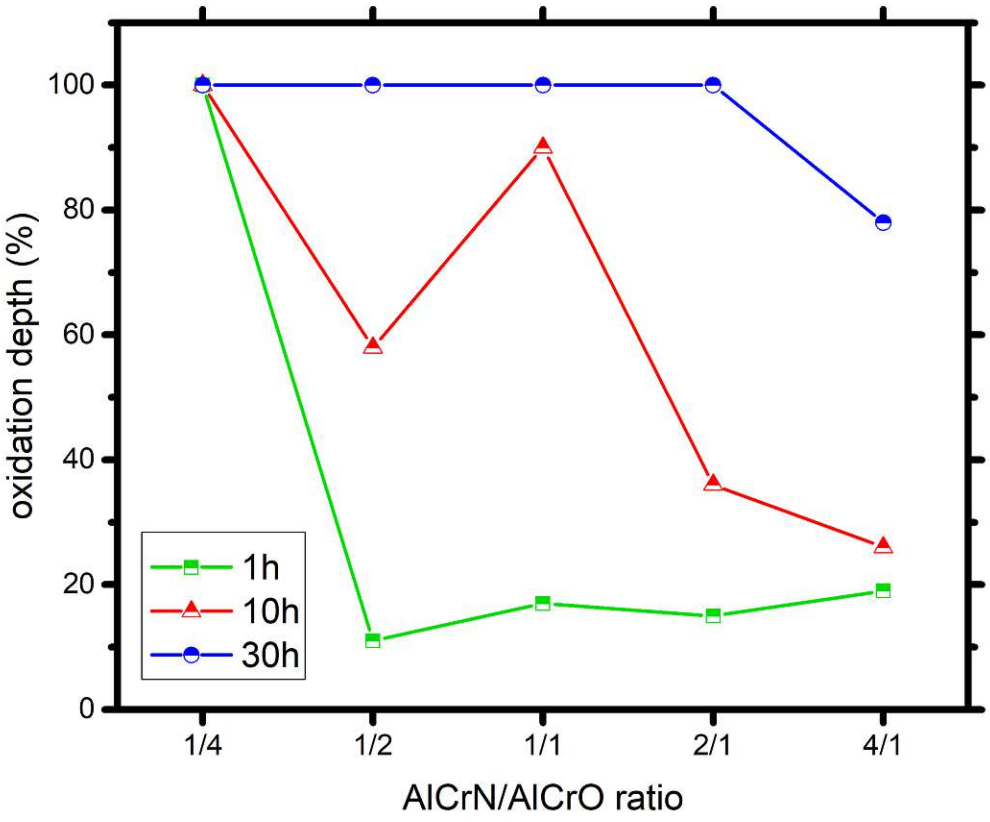

Figure 3.15: Diagram of the resulting oxidation depth of all coatings for exposure of 1 h, 10 h and 30 h, respectively

Chapter 4

Conclusion

Summarizing the experimental data collected with the various oxidation tests, we notice that the gathered information is not coherent in itself, but rather affected by the method used to investigate the high temperature corrosion stability. Depending on the testing conditions, we get two conflictive statements, that gainsay each other. While the DSC-experiments showcased that higher oxidation stability can be obtained by using higher oxygen content coatings, the furnace annealing testing procedure using samples in as deposited state tells us that the oxidation stability is, in fact, the lowest for the high oxygen content coatings, while the high nitrogen content coatings can withstand elevated temperatures much longer. The reason for this discrepancy has to be situated in the way samples are prepared for each test. While the DSC procedure requires the coating be ground to powder, the furnace test was carried out using sapphire substrate samples with the coating in as deposited state. Due to the much higher surface the powdery sample exposes, the influence of the layered architecture is not conveyed perfectly into the testing. The big surface allows the oxidation to advance much faster than it normally would, particularly exposing the nitrogen-rich parts to accelerated decomposition. As the nitrogen content in the high oxygen content coating is much lower by default, much less of the total sample mass can be oxidized, thus leading to a seemingly more stable behaviour of the coating. The results, however, do not prove that the desired effect of shielding the nitrogen layers against high temperature corrosion with alternating oxide layers can be increased with higher oxygen content. The furnace annealing test, on the other hand, is much closer to the actual real live application of the coating and also - by and large - only has contact to the oxidizing agent with one surface, allowing the desired shielding effect to be thoroughly tested. As the results show us, higher oxygen content does not increase the shielding effect in this setting. Quite on the contrary, the lower the oxygen content is, the better the coating's oxidation resistance gets. The reason behind this behaviour probably has to be attributed to the lower density of the high oxygen content coating due to the different morphologies of the contributing materials. These discrepancies cause less dense interface structures and allow for the existence of more imperfections

and defects, leading to an overall higher diffusivity for high oxygen coatings. Especially the aforementioned (sec. 3.1.2) higher droplet inclusion rate for AlCrO coatings produced by arc evaporation, which leads to an increased number of fast diffusion pathways, can contribute to this effect. This means that high oxygen coatings not only don't provide better shielding effect than lower oxygen content coatings, but also even further decrease the oxidation resistance by making faster diffusive pathways available for oxygen molecules. However, it is not clear as of now that the shielding by application of oxygen layers doesn't work at all. As no tests with pure AlCrN multilayer coatings were carried out for this study, a positive effect of the application of very thin AlCrO layers cannot be excluded.

Undeniably, this study also points out that the right choice of testing procedures is crucial for achieving results that are applicable to real live behaviour. According to the data presented in this thesis, it is at least debatable if DSC analysis is a suitable method to investigate the thermal stability and oxidation resistance of coatings with multilayer architecture, as the influence of this architecture is obviously decreased by the requirements of sample preparation. Especially for systems with layers of different substances, such as the investigated AlCrN/ AlCrO multilayer arrangement, DSC analysis may not deliver results that adequately represent the behaviour in real life applications.

Chapter 5

Summary

The scope of this thesis was to investigate, if an architecture consisting of alternating AlCrN and AlCrO layers could increase the thermal stability and oxidation resistance of cutting tool thin film coatings. The examined specimen were deposited via PVD and were built up from 80 bilayer periods of alternating AlCrN and AlCrO. Five different chemical compositions were selected and a multitude of different tests were carried out, starting with DSC tests in He atmosphere to gather data on the thermal stability of the different coatings. Here, the low nitrogen coatings with N:O ratio 1:2 and 1:4 showed superior results than the other coatings. The same pattern could be observed during the second testing procedure, where DSC analyses in synthetic air were carried out. Based on these data and additional mechanical tests, the coating with N:O ratio 1:2 was selected as most promising candidate. With this coating, we now carried out long-term DSC analyses at 4 different temperatures in synthetic air, to determine which treatment the coating at best could endure. It was discovered that the maximum temperature the coating could withstand for 5 h without completely decomposing was around $1000°C$. Therefore, the next experiment, where samples of each architecture were annealed in a furnace, was conducted at $1000°C$. Always after $1, 10$ and 30 h, one of each sample type was taken out of the furnace and prepared for further investigation at the SEM, where EDX line scans were performed to identify the chemical composition of the coating versus the coating thickness. The data obtained during this experiment completely contradicted all the experimental evidence gathered thus far, as the high nitrogen content coatings outperformed the high oxygen content coatings effortlessly. As these last tests represented the most realistic experimental procedure in regard to the later application as tool coating, the imposing conclusion is that all the data gathered before is not applicable to real live uses of the designed coatings. This means that, considering the final results, raising the AlCrO ratio in AlCrN/AlCrO multilayer coatings does not increase the oxidation resistance, but in fact lowers it due to the introduction of defects in the interfaces and layer morphology, which serve as high diffusivity pathways for oxygen. Especially the higher density of droplet inclusions in the coating, which is an intrinsic draw-

back of AlCrO coatings prepared by arc evaporation, has to be considered here. However, the results do not confirm once and for all that the AlCrN/AlCrO system can not be used for improving overall high temperature stability. It is still possible that a single or maybe even multiple compositions with better properties than coatings with other AlCrN/AlCrO ratios exist, even though the results of this study make this more unlikely. Furthermore, this thesis challenges the use of DSC analyses as the primary tool to investigate the thermal stability and oxidation resistance of multilayer coatings. While DSC-TGA systems provide potent tools to examine the properties of coatings and the decomposition process at high temperatures, the obtained data concerning the actual resistance against high temperature corrosion seems to contain very few to no data usable for real applications. Here, testing procedures employing the coatings in their as deposited state serve as a far more reliable source of information.

Appendix

SEM- images and line scans

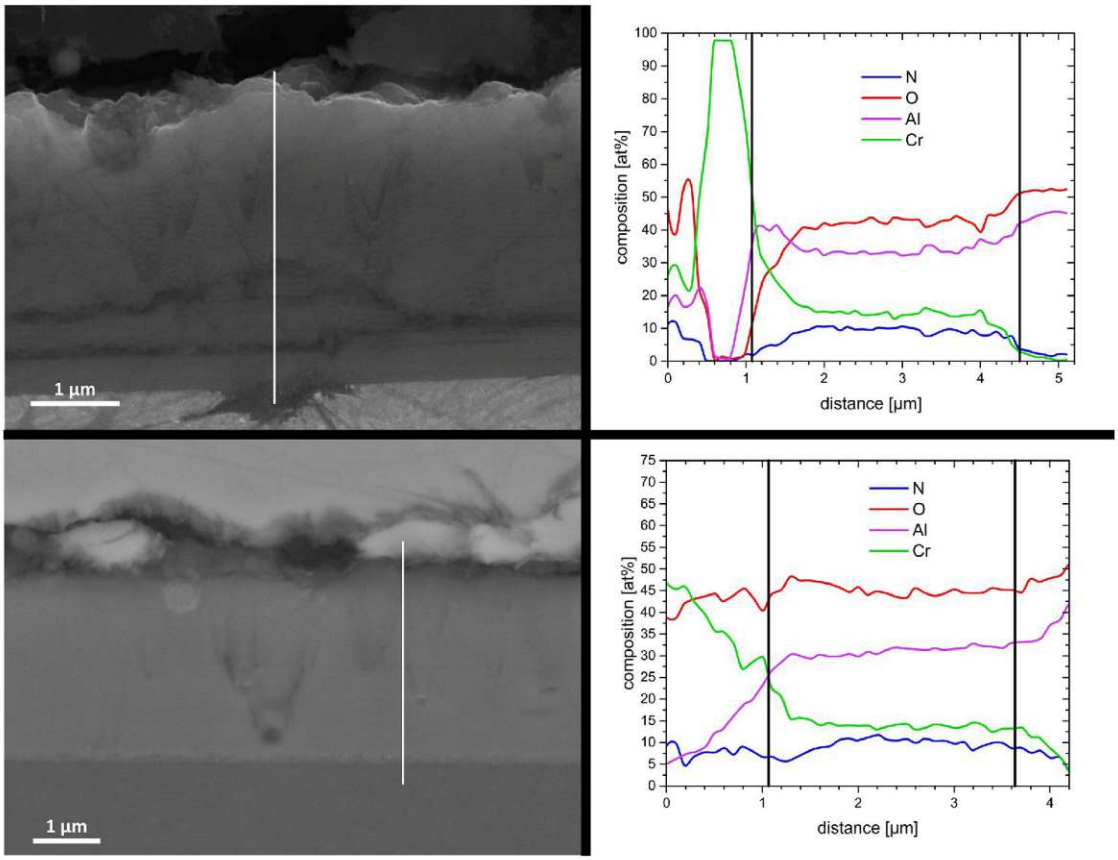

Figure 5.1: SEM- images and EDX line scan results for the N:O 1:1 coating; top: as deposited state; bottom: after 1 h of annealing at 1000°C; the white line specifies the line scan position; the two black lines in the diagram define the borders of the multilayer coating

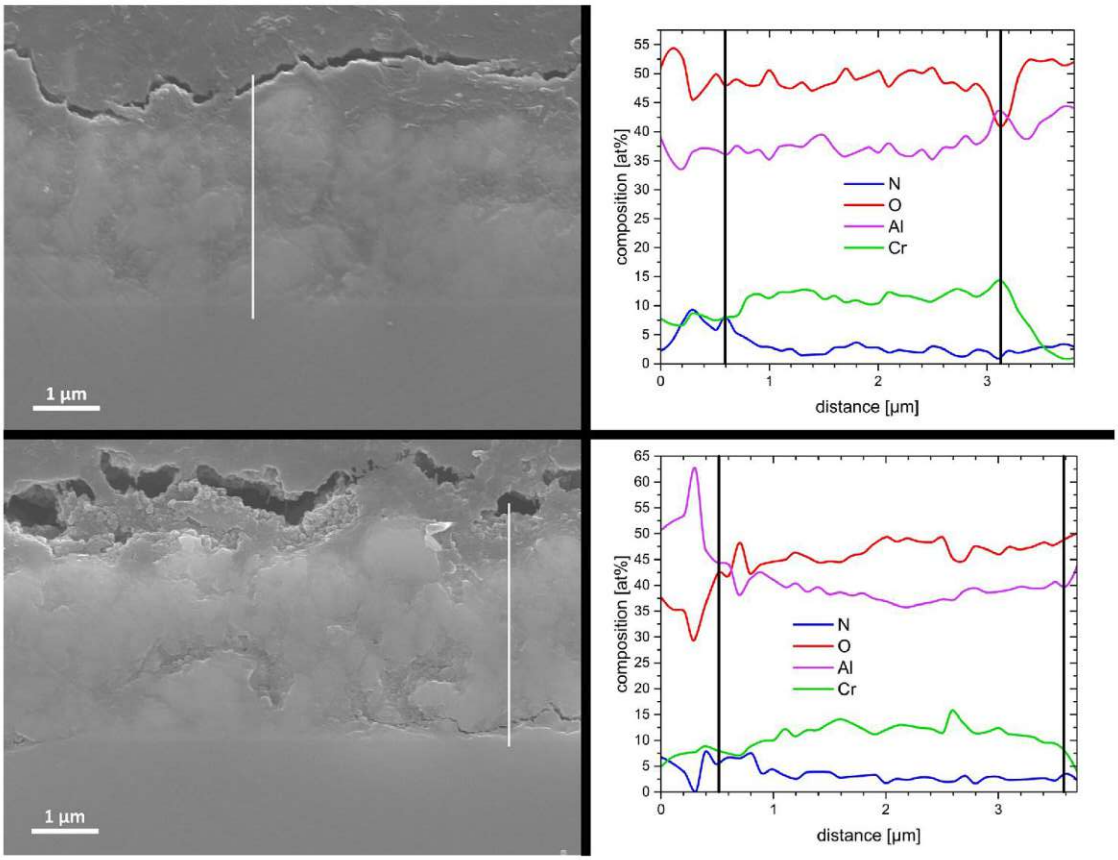

Figure 5.2: SEM- images and EDX line scan results for the N:O 1:1 coating; top: after 10 h of annealing at 1000°C; bottom: after 30 h of annealing at 1000°C; the white line specifies the line scan position; the two black lines in the diagram define the borders of the multilayer coating

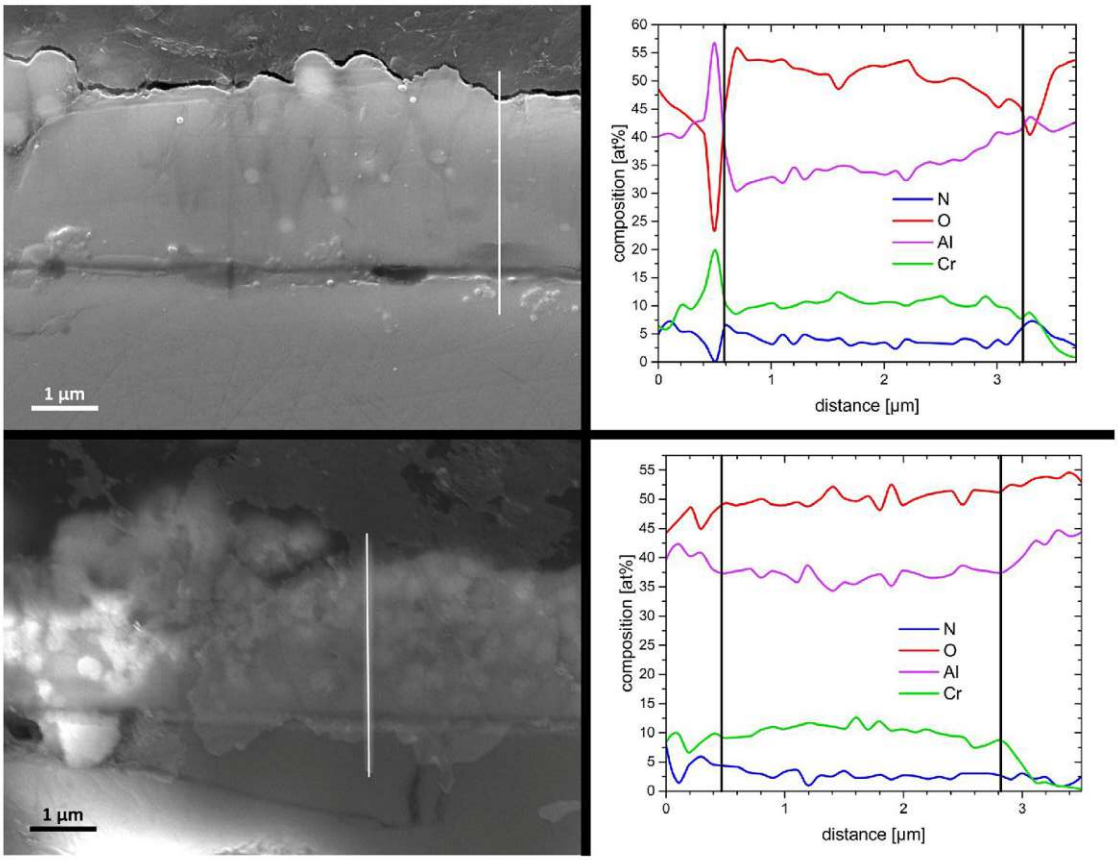

Figure 5.3: SEM- images and EDX line scan results for the N:O 1:4 coating; top: as deposited state; bottom: after 1 h of annealing at 1000°C; the white line specifies the line scan position; the two black lines in the diagram define the borders of the multilayer coating

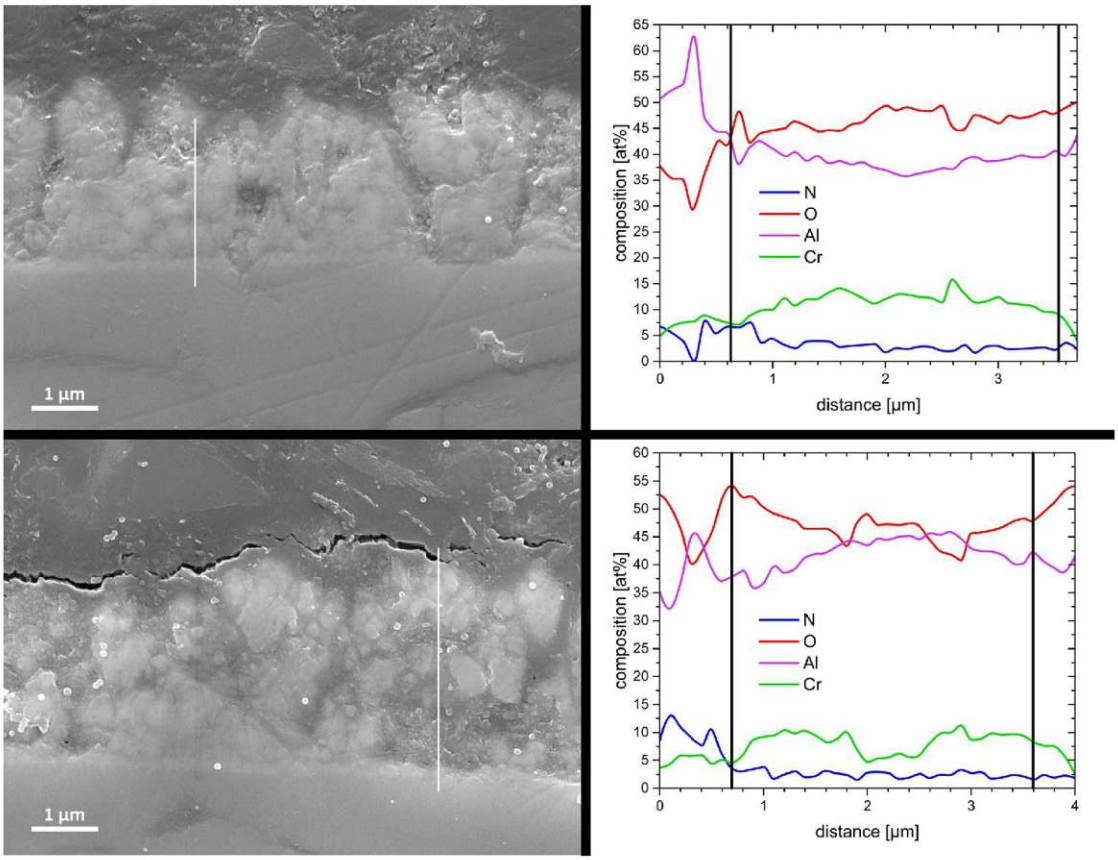

Figure 5.4: SEM- images and EDX line scan results for the N:O 1:4 coating; top: after 10 h of annealing at 1000°C; bottom: after 30 h of annealing at 1000°C; the white line specifies the line scan position; the two black lines in the diagram define the borders of the multilayer coating

Bibliography

[1] M. Miller, G. Mulholland, and C. Anderson, Journal of Manufacturing Science and Engineering (2003).

[2] A. Markopoulos and M. D.E., Journal of Manufacturing Technology Research (2010).

[3] H. Riedl, "sputtern-plasma-1," TU Wien.

[4] C. Koller, *Triggering the Phase Evolution within TiAlN- and (Al,Cr)2O3-based Hard Coatings by Alloying and Microstructural Concepts*, Ph.D. thesis, TU Wien (2015).

[5] R. Bürgel, H. Maier, and T. Niendorf, *Handbuch Hochtemperatur- Werkstofftechnik* (Vieweg+ Teubner Verlag, Wiesenbaden, Deutschland, 1998).

[6] P. Mayrhofer, *Material Science* (TU Wien, Wien).

[7] A. Kirnbauer, "Impact of fe on the oxide phase formation and oxidation behaviour of cathodic arc evaporated al-cr films," TU Wien (2017).

[8] P. Mayrhofer, *Materials Science of Metallic Materials* (TU Wien, Wien, 2016).

[9] P. Mayrhofer, *Surface Technology* (TU Wien, Wien, 2016).

[10] R. Raab, *Architecturally-designed Al-Cr-based nitride/oxide and oxynitride coatings for high temperature applications*, Ph.D. thesis, TU Wien (2017).

[11] F. Klocke and W. König, *Fertigungsverfahren Drehen, Fräsen, Bohrne* (Springer Verlag, Berlin Heidelberg New York, 2008).

[12] A. Kalweit, C. Paul, S. Peters, and R. Wallbaum, *Handbuch für Technisches Produktdesign* (Springer Verlag, Berlin Heidelberg New York, 2012).

[13] W. Weißbach, *Werkstoffkunde* (Springer Verlag, Berlin Heidelberg New York, 2010).

[14] R. Raab, C. Koller, S. Kolozsvári, J. Ramm, and P. Mayrhofer, ELSEVIER (2017).

[15] P. Mayrhofer, *Werkstoffkunde metallischer Werkstoffe* (TU Wien, Wien, 2016).

[16] A. Inspektor and P. Salvador, ELSEVIER (2014).

[17] G. Blasek and G. Bräuer, *Vakuum Plasma Technologien* (Eugen G. Leuze Verlag, Bad Saulgau, Deutschland, 2010).

[18] K. Oura, V. Lifshits, A. Saranin, A. Zotov, and M. Katayama, *Surface Science* (Springer Verlag, Berlin Heidelberg New York, 2003).

[19] R. Baluffi, S. Allen, and W. Carter, *Kinetics of Materials* (John Wiley and Sons, Inc., Hoboken, New Jersey, 2005).

[20] R. Hollerweger, *The Role of Tantalum on Structure, Thermal Stability, and Oxidation Resistance of Ti-Al-N and Cr-Al-N Coatings*, Ph.D. thesis, TU Wien (2013).

[21] J. Goldstein, D. Newbury, D. Joy, J. Michael, N. Ritchie, and J. Scott, *Scanning electron microscopy and x-ray microanalysis* (Springer verlag, New York, New York, 2017).

[22] W. Kalss, A. Reiter, V. Derflinger, C. Gey, and J. Endrino, ELSEVIER (2005).

[23] I. Petrov, P. Barna, L. Hultman, and G. J.E., Journal of Vacuum Science I& Technology A: Vacuum, Surfaces, and Films (2003).

[24] S. Noda, K. Tepsanongsuk, Y. Tsuji, Y. Kajikawa, Y. Ogawa, and H. Komiyama, Journal of Vacuum Science I& Technology A: Vacuum, Surfaces, and Films (2004).

[25] P. Mayrhofer, M. Geier, C. Löcker, and L. Chen, International Journal of Materials Research (2009).

[26] H. Holleck, Journal of Vacuum Science I& Technology A: Vacuum, Surfaces, and Films (1985).

[27] P. Y. Hou, A. Paulikas, B. Veal, and J. Smialek, ELSEVIER (2007).

[28] C. Shin, Y. Kim, D. Gall, J. Greene, and I. Petrov, ELSEVIER (2002).

[29] Z. Zhang, *Impact of Al on Structure and Mechanical Properties of NbN and TaN*, Ph.D. thesis, Montanuniversität Leoben (2011).